MOLECULAR BIOLOGY

Gliotoxin, identified from a screen of fungal metabolites, disrupts 7SK snRNP, releases P-TEFb, and reverses HIV-1 latency

Mateusz Stoszko[1], Abdullah M. S. Al-Hatmi[2,3,4]*, Anton Skriba[5]*, Michael Roling[1]*, Enrico Ne[1]*, Raquel Crespo[1]*, Yvonne M. Mueller[6]*, Mohammad Javad Najafzadeh[2,7]*, Joyce Kang[8], Renata Ptackova[5], Elizabeth LeMasters[1], Pritha Biswas[1], Alessia Bertoldi[1,9], Tsung Wai Kan[1], Elisa de Crignis[1], Miroslav Sulc[5], Joyce H.G. Lebbink[10], Casper Rokx[11], Annelies Verbon[11], Wilfred van Ijcken[12], Peter D. Katsikis[6], Robert-Jan Palstra[1], Vladimir Havlicek[5], Sybren de Hoog[2,3], Tokameh Mahmoudi[1†]

A leading pharmacological strategy toward HIV cure requires "shock" or activation of HIV gene expression in latently infected cells with latency reversal agents (LRAs) followed by their subsequent clearance. In a screen for novel LRAs, we used fungal secondary metabolites as a source of bioactive molecules. Using orthogonal mass spectrometry (MS) coupled to latency reversal bioassays, we identified gliotoxin (GTX) as a novel LRA. GTX significantly induced HIV-1 gene expression in latent ex vivo infected primary cells and in CD4$^+$ T cells from all aviremic HIV-1$^+$ participants. RNA sequencing identified 7SK RNA, the scaffold of the positive transcription elongation factor b (P-TEFb) inhibitory 7SK small nuclear ribonucleoprotein (snRNP) complex, to be significantly reduced upon GTX treatment of CD4$^+$ T cells. GTX directly disrupted 7SK snRNP by targeting La-related protein 7 (LARP7), releasing active P-TEFb, which phosphorylated RNA polymerase II (Pol II) C-terminal domain (CTD), inducing HIV transcription.

INTRODUCTION

Combination antiretroviral therapy (cART) causes a drastic and immediate viral decrease by targeting distinct steps in the HIV-1 life cycle, effectively blocking replication and halting disease progression (*1*–*3*). However, cART does not target or eliminate HIV that persists in a latent state in cellular reservoirs. Because some of the proviruses are replication competent, latent HIV-infected cells inevitably rebound once cART is interrupted, leading to necessity for lifelong therapy (*4*). Particularly in resource-limited countries, which are also disproportionally affected, this is translated into an insurmountable medical, social, and financial burden. To achieve a scalable cure for HIV infection, it will be necessary to reduce or eliminate the latent HIV-infected reservoir of cells and/or equip the immune system with the robustness and effectiveness necessary to prevent viral rebound such that cART can be safely discontinued.

An important breakthrough in HIV-1 cure was the unequivocal proof that it is possible to mobilize the latent patient HIV reservoir by treatment with agents that activate HIV gene expression [latency reversal agents (LRAs)] (*5*). However, clinical studies thus far have shown little to no reduction in the latent reservoir in patients (*6*, *7*). This is consistent with limited potency and specificity of currently tested drugs, which appear to be unable to reach a significant proportion of latently infected cells or to induce HIV-1 expression in latent reservoir at sufficient levels to produce viral proteins for recognition by the immune system (*8*). Furthermore, transcriptional stochasticity and heterogeneity of latent HIV integrations (*9*) may pose additional barriers to reactivation of the latent reservoir as a whole; sequential rounds of stimulation yield new infectious particles (*10*), while certain LRA combinations result in more efficient latency reversal when administered in intervals rather than at once (*11*). In addition, pleiotropic functions and toxic effects of LRAs may compromise the ability of CD8$^+$ T cells to eliminate HIV protein–expressing cells (*12*, *13*). Therefore, it is critical to identify and develop novel therapeutics, which strongly induce HIV-1 gene expression to effectively disrupt HIV latency without dampening the immune response.

The pharmaceutical industry is highly equipped for high-throughput screens using defined synthetic libraries. While this is an effective approach, it is important to record that approximately half of the novel small molecules introduced to the market between 1981 and 2014 are natural or nature-derived (*14*). Biological systems represent an invaluable source of functional molecules with high chemical diversity and biochemical specificity, evolved during millions of years of adaptation. In particular, fungi represent a largely unexplored source of compounds with potential therapeutic use. Fungi secrete a gamut

[1]Department of Biochemistry, Erasmus MC University Medical Center Rotterdam, PO Box 2040, 3000 CA Rotterdam, Netherlands. [2]Westerdijk Fungal Biodiversity Institute, Utrecht, Netherlands. [3]Center of Expertise in Mycology of Radboud UMC/CWZ, Nijmegen, Netherlands. [4]Ministry of Health, Directorate General of Health Services, Ibri, Oman. [5]Institute of Microbiology of the Czech Academy of Sciences, Videnska 1083, CZ 14220 Prague 4, Czech Republic. [6]Department of Immunology, Erasmus MC University Medical Center Rotterdam, PO Box 2040, 3000 CA Rotterdam, Netherlands. [7]Department of Parasitology and Mycology, Faculty of Medicine, Mashhad University of Medical Sciences, Mashhad, Iran. [8]Key Laboratory of Environmental Pollution Monitoring/Disease Control, Ministry of Education and Guizhou Talent Base of Microbes and Human Health, School of Basic Medicine, Guizhou Medical University, Guiyang 550025, P. R. China. [9]Microbiology Section, Department of Experimental, Diagnostic and Specialty Medicine, School of Medicine, University of Bologna, Bologna, Italy. [10]Departments of Molecular Genetics and Radiation Oncology, Erasmus University Medical Center, PO Box 2040, 3000 CA Rotterdam, Netherlands. [11]Department of Internal Medicine, Section of Infectious Diseases, Erasmus University Medical Center, PO Box 2040, 3000 CA, Rotterdam, Netherlands. [12]Erasmus MC Genomics Core Facility, Department of Cell Biology, Erasmus University Medical Center, PO Box 2040, 3000 CA, Rotterdam, Netherlands.
*These authors contributed equally to this work.
†Corresponding author. Email: t.mahmoudi@erasmusmc.nl

of extracellular compounds and other small molecular extrolites (*15*). While some of these compounds have been shown to have antibiotic (ex. penicillin) or carcinogenic (ex. aflatoxin) properties, little is known in general about their biological activities and possible molecular targets. In addition, a single fungal strain often produces a wide array of secondary metabolites that are not essential for its growth but are exuded as a consequence of specific environment, such as nutrient-rich versus minimal growth conditions (*16*, *17*). Fungal extrolites might target various signaling pathways in mammalian cells, such as those influencing HIV-1 gene expression. Fungal supernatants are an ideal source for an expert academic setting, where low- and medium-throughput biological screening systems, academic knowledge of evolutionary mycology, and state-of-the-art fractionation and purification techniques are routinely combined. Studies of regulation of HIV-1 gene expression have identified distinct molecular mechanisms and cellular pathways at play, which can be targeted pharmacologically to activate expression of latent HIV (*18*, *19*). The rich diversity of fungal extrolites therefore may prove an untapped source of new compounds that target HIV for reactivation. In search of novel LRAs, here, we have performed an unbiased medium-throughput screen of fungal extrolites, coupled to HIV latency reversal bioassays and orthagonal fractionation and mass spectrometry (MS)/nuclear magnetic resonance (NMR), and identified gliotoxin (GTX). GTX potently reversed HIV-1 latency in multiple in vitro latency models as well as ex vivo in cells obtained from all aviremic HIV-1–infected patients examined without associated cytotoxicity. We demonstrate that GTX disrupts the positive transcription elongation factor (P-TEFb)–sequestering 7SK small nuclear ribonucleoprotein (snRNP) complex by targeting the La-related protein 7 (LARP7) component, leading to degradation of its scaffold 7SK RNA and release of active P-TEFb, which is then recruited by Tat to phosphorylate the Ser^2 residue of the RNA polymerase II (Pol II) C-terminal domain (CTD) and activate HIV transcription elongation. Our data highlight the power of combining a medium-throughput bioassay, mycology, and orthogonal MS to identify novel potentially therapeutic compounds.

RESULTS

Growth supernatant of *Aspergillus fumigatus* identified in a medium-throughput screen of fungal secondary metabolite has HIV-1 latency reversal activity

We screened 115 species of filamentous fungi for their ability to induce HIV-1 proviral expression; of the species that appeared promising, 2 to 4 additional strains were tested (table S1). The species belonged to 28 orders (43 families) of the fungal kingdom (Fig. 1A) and were chosen on the basis of their evolutionary position, ecological trends, and known active production of extracellular compounds. The majority of fungi were of ascomycetous affinity, four species were of basidiomycetous affinity, and two belonged to the lower fungi. Selected fungi were grown in both complete yeast media and minimal media (RPMI 1640), as they are known to produce distinct extrolites depending on their growth conditions (fig. S1). Culture supernatants were then screened for latency reversal activity using Jurkat-derived 11.1 and A2 cell line models of HIV-1 latency (J-Lat) in a low-medium throughput assay setup, in which expression of green fluorescent protein (GFP) is controlled by the HIV-1 promoter and indicates latency reversal. We identified the supernatant of *Aspergillus fumigatus* CBS 542.75 to strongly activate the latent HIV-1 5′ long terminal repeat (LTR) (Fig. 1B). We also compared other *Aspergillus* species growth supernatants indicated for their potential to induce HIV-1 expression (Fig. 1C) and observed that only strains of *A. fumigatus* (CBS 542.75, CBS 113.26, and CBS 100074) had latency reversal activity (Fig. 1C).

Orthogonal liquid chromatography–MS/NMR strategy coupled to latency reversal bioassays identifies GTX from growth supernatant of *A. fumigatus* as a putative LRA

Because of the chemical complexity of the positive fungal supernatants, direct MS analysis of their constituents proved to be impossible. Therefore, *A. fumigatus* CBS 100074 growth supernatant was fractionated several times by means of orthogonal MS (Fig. 1D). We selected this particular supernatant as it showed the highest potency to reverse latency in the J-Lat models. After each round of fractionation, all samples/fractions were again tested in latency reversal bioassays, followed by quantitation of the GFP expression and identification of fractions retaining latency reversal activity. As expected, originally less active fractions became more active during the fractionation/enrichment process (Fig. 1E). The most active 7B/7C fractions were further fractioned on a hydrophilic-lipophilic balance (HLB) cartridge (11 samples) and components of 7B/7C and 11C fractions dereplicated by CycloBranch software (Fig. 1E and fig. S2, A and B) (*20*). Compound matching against the annotated database of *Aspergillus* secondary metabolites revealed a set of candidate compounds further selected for latency reversal testing (fig. S2C and table S2). Among the candidate molecules identified, GTX, obtained from a commercially available synthetic source, was able to induce expression of the latent provirus in a concentration-dependent manner (Fig. 1F). Notably, GTX was found in all positive fractions (table S2). While GTX isolated from supernatant of CBS 100074 showed strong induction of HIV-1 transcription, supernatant of *Aspergillus flavus* (CBS 625.66), a close relative of *A. fumigatus* that was inactive in latency reversal (Fig. 1C), did not contain GTX (fig. S2, D and E), providing further support that GTX is the main mediator of LRA activity in *A. fumigatus* supernatants.

GTX reverses latency in ex vivo infected primary $CD4^+$ T cells without associated cytotoxicity

To examine the latency reversal potential of GTX in a more clinically relevant system, we used a modified primary ex vivo infected latency model, in which primary $CD4^+$ T cells are infected with a full-length replication-incompetent HIV-1 virus driving expression of the luciferase reporter (fig. S3A) (*21*). Treatment of latently infected $CD4^+$ T cells with GTX resulted in significant, concentration-dependent latency reversal at lower concentrations than necessary to achieve reactivation in latently infected cell lines (Fig. 2, A to C). GTX (20 nM) treatment resulted in more than 20-fold induction of HIV-1 expression (Fig. 2A), which translated into more than 10% latency reversal of that observed upon maximal stimulation with phorbol 12-myristate 13-acetate (PMA)/ionomycin (Fig. 2B). Similar to the latency reversal observed using commercially available synthetic GTX (Fig. 2, A and B), treatment of HIV-1–infected latent primary $CD4^+$ T cells with GTX isolated from growth supernatant of *A. fumigatus* CBS 100074, estimated at 20 nM by NMR in comparison to commercially available GTX, resulted in significant latency reversal, approximately 10% of maximal PMA/ionomycin stimulation (Fig. 2C). At high concentrations, GTX is known to be toxic to immune cells (*22*–*24*), ascribed to its unusual disulfide

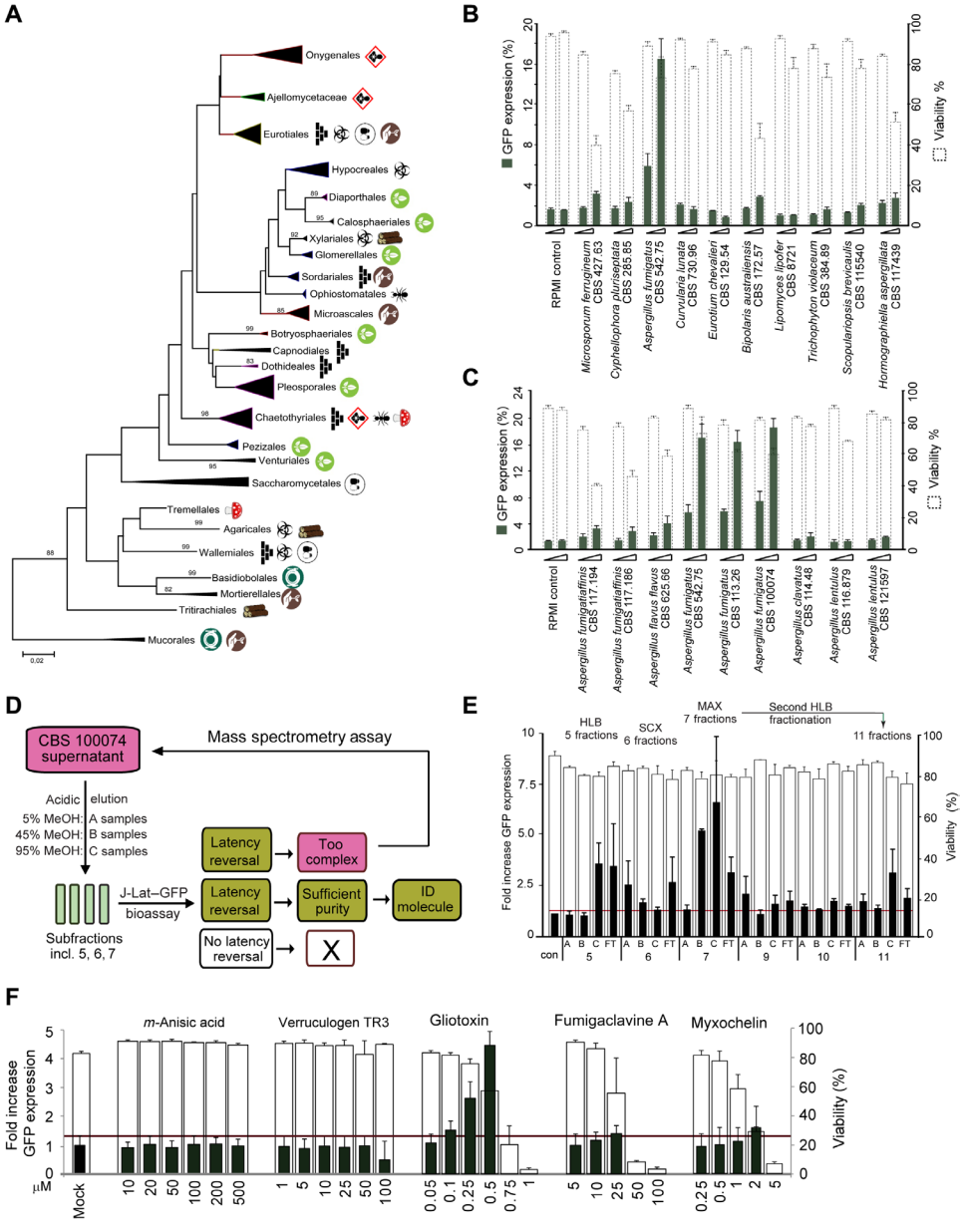

Fig. 1. Medium-throughput screen of fungal secondary metabolites combined with orthogonal fractionation and MS strategy coupled to latency reversal bioassays identifies GTX from growth supernatant of *A. fumigatus* to reverse HIV-1 latency. (**A**) Phylogenetic tree representing the main orders of the fungal kingdom with strains used in the current study, collapsed per order. Orders selected from the tree published (*57*), with some of the lower orders included for structural reasons. Approximate ecological trends in the orders are summarized by symbols, as follows: vertebrate pathogenicity prevalent, climatic extremotolerance prevalent, frequent production of extracellular metabolites or mycotoxins, frequent osmotolerance or growth in sugary fluids, numerous members with soilborne lifestyle, numerous members inhabiting decaying wood rich in hydrocarbons, frequent insect association, frequent mushroom decomposition or hyperparasitism on fungi or lichens, and frequent inhabitants of foodstuffs or vertebrate intestinal tracts. (**B**) Latency reversal bioassay performed by treatment of J-Lat A2 cells with increasing volumes of growth [normalized by O.D. (optical density)] supernatants obtained from selected fungal strains. (**C**) Latency reversal bioassay in J-Lat A2 cells with growth supernatants obtained from members of the *Aspergillus* genus. Cells were treated as in (B). (**D**) Schematic representation of the orthogonal MS strategy coupled to latency reversal bioassays used to identify putative LRA. See main text for full description. (**E**) Three preconcentration cartridges (HLC, SCX, and MAX) were combined with variable content of extracting solvent (A: 5% MeOH, B: 45% MeOH, and C: 95% MeOH; FT, flowthrough). Latency reversal potential of fractionated secondary fungal metabolites was tested via treatment of J-Lat A2 cells. Latency reversal (fold increase percentage of GFP, left axis, black bars) and cell viability (percentage of viability, right axis, empty bars) were assessed by flow cytometry analysis. (**F**) Commercially obtained versions of five common molecules identified in active fractions were tested for LRA activity in J-Lat A2 cells. Data are presented as fold increase percentage of GFP expression and percentage of viability as indicated, ±SD from at least three independent experiments.

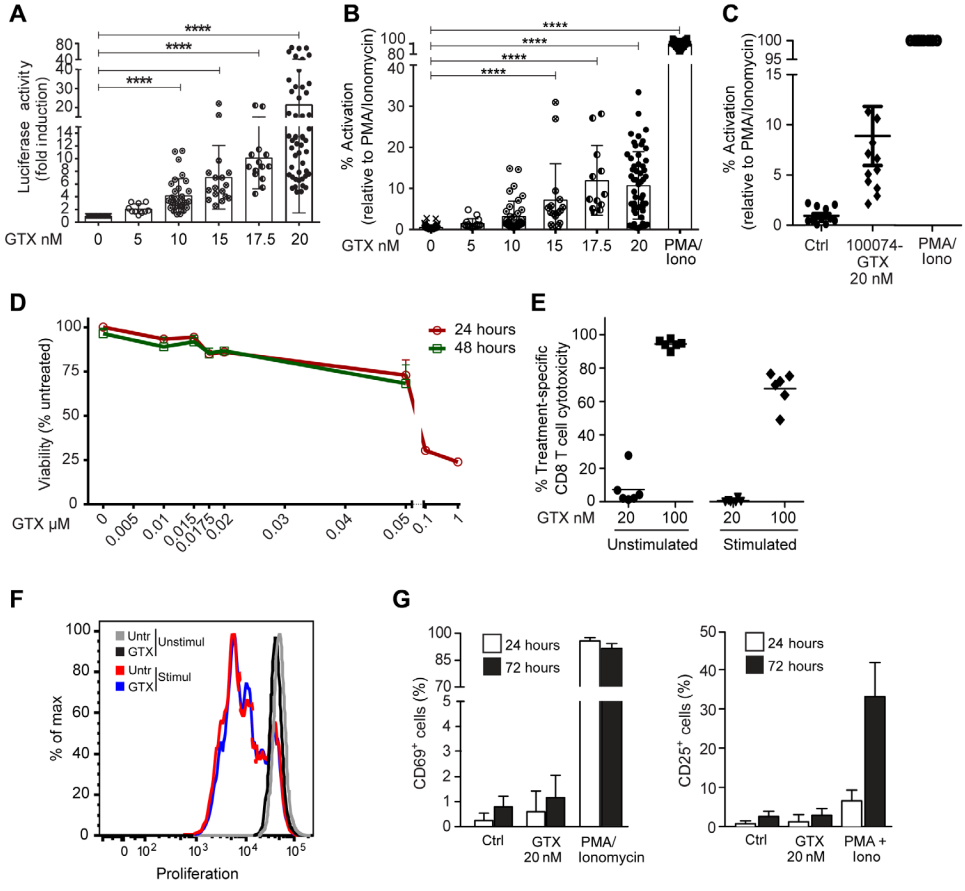

Fig. 2. GTX (20 nM) reverses HIV-1 latency in ex vivo infected primary CD4$^+$ T cells without associated cytotoxicity, T cell activation, or inhibition of proliferative capacity. (**A**) Latency reversal after treatment of latently infected primary CD4$^+$ T cells with increasing concentrations of GTX for 24 hours as indicated, shown as fold induction over untreated control luciferase activity. Statistical analysis was calculated using Kruskal-Wallis one-way analysis of variance (ANOVA) (****$P < 0.0001$). (**B**) Data presented in (A) normalized and shown as percent latency reversal activity relative to treatment with PMA/Ionomycin. (**C**) Latency reversal after treatment of HIV-1–infected latent primary CD4$^+$ T cells with 20 nM GTX isolated from growth supernatant of *A. fumigatus* CBS 100074, measured as increased luciferase activity normalized to and shown as percentage of activation of PMA/ionomycin ($n = 6$). Wide horizontal lines represent average, and shorter horizontal lines represent SD. (**D**) Viability of the primary CD4$^+$ T cells treated for 24 (red line) and 48 (green line) hours with indicated increasing concentrations of GTX, assessed by flow. (**E**) Unstimulated or αCD3/αCD28-stimulated PBMCs were treated with 20 and 100 nM GTX for 72 hours, stained with AnnexinV, and cell death (AnnexinV$^+$ CD3$^+$CD8$^+$) was determined by flow cytometry. Treatment-specific cell cytotoxicity was calculated as indicated in the Materials and Methods section. Each symbol represents one healthy donor ($n = 6$), and horizontal lines depict means. (**F**) Representative fluorescence-activated cell sorting (FACS) plot overlay showing the proliferation of unstimulated or αCD3/CD28-stimulated CD8$^+$ T cells in the presence or absence of GTX. Cells were stained with a proliferation dye and analyzed 72 hours later by flow cytometry to define nonproliferating cells (proliferation dye undiluted, bright stain intensity) and dividing cells (proliferation dye diluted, reduced stain intensity). (**G**) Activation status of primary CD4$^+$ T cells upon GTX treatment as indicated ($n = 6$).

bridge, and responsible for pleiotropic effects on cellular and viral systems (*25*).

Consistent with the literature, GTX concentrations upward of 100 nM induced significant toxicity as indicated by annexin V staining (Fig. 2D and fig. S3B). However, primary CD4$^+$ T cell viability was not significantly affected after GTX treatment at concentrations up to 20 nM, with moderate toxicity observed at 50 nM (Fig. 2D and fig. S3B). Thus, at lower concentrations in which GTX did not show toxicity on CD4$^+$ T cells, strong latency reversal was induced (Fig. 2, A to D, and fig. S3B). CD8$^+$ T cells play a central role in eliminating HIV-infected cells (*26*). Therefore, it is of utmost importance to evaluate the potential toxicity of newly developed LRAs on CD8$^+$ T cells (*13*). GTX at a low concentration of 20 nM did not reduce the viability or proliferation capacity of CD8$^+$ T cells whether unstimulated or αCD3/αCD28-stimulated peripheral blood mononuclear cells (PBMCs) were examined (Fig. 2, E and F, and fig. S4, A and B). Consistent with the literature (*22*–*25*), treatment with higher concentrations of GTX at 100 nM and 1 µM caused apoptosis and death of primary CD4$^+$ and CD8$^+$ T cells as well as B cells, natural killer (NK) cells, and monocytes, as shown by annexin V staining followed by flow cytometry (Figs. 2, D and E, and 3C and figs. S3B and S4, A to C). Potential for clinical applicability of a candidate LRA also requires that it does not induce global T cell activation nor should it interfere with CD8$^+$ T cell activation. Treatment of unstimulated primary CD4$^+$ T cells and CD8$^+$ T cells with GTX (20 nM), which significantly reversed latency, did not induce expression of the T cell activation markers CD69 and CD25 (Figs. 2G and 3D and fig. S5, A and B), nor did it induce proliferation of resting CD4$^+$ and CD8$^+$ T cells (fig. S5, C and D), while, as expected, PMA/ionomycin treatment activated T cells (Fig. 2G). Conversely, GTX treatment of activated PBMCs also did

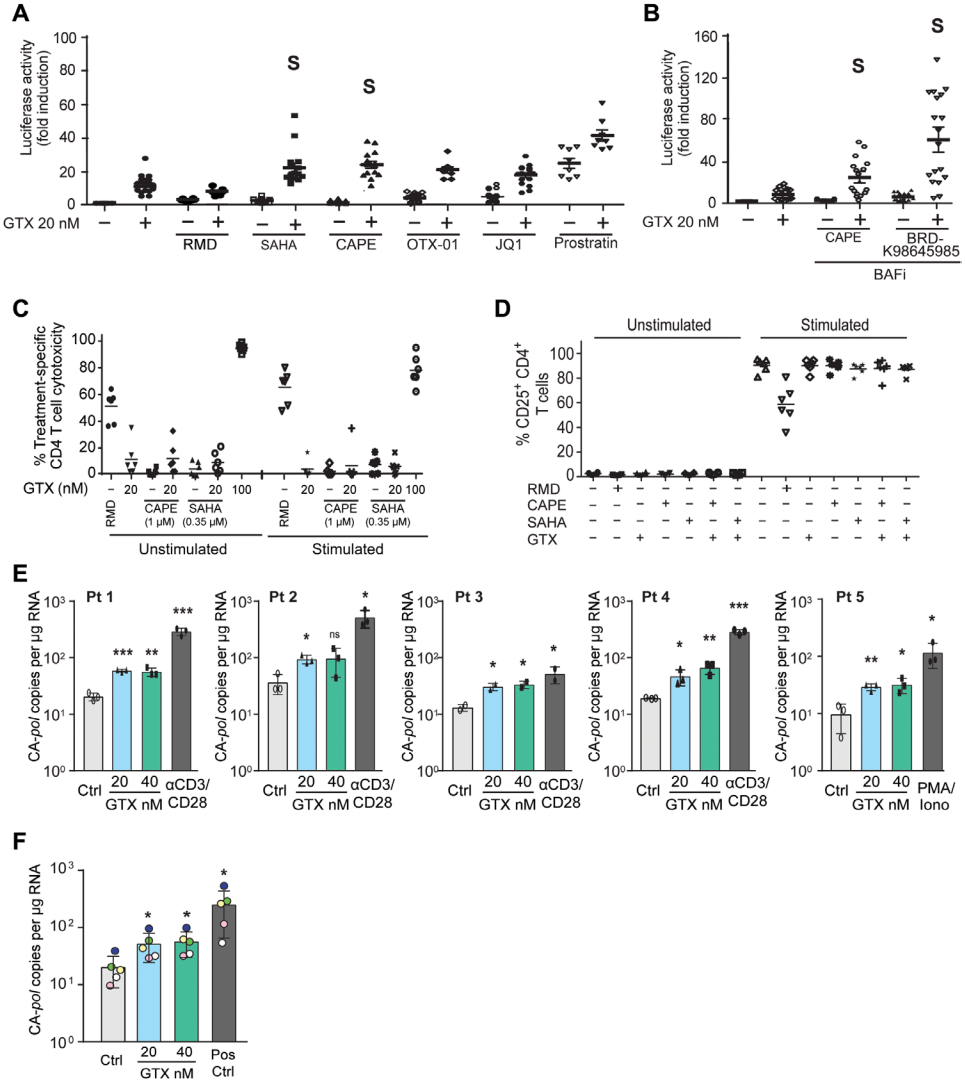

Fig. 3. GTX strongly synergizes with HDAC and BAF inhibitors and reverses latency in primary CD4$^+$ T cells obtained from all tested aviremic participants. (**A** and **B**) HIV-1 latency reversal in latent ex vivo HIV-1–infected primary CD4$^+$ T cells in response to 24-hour cotreatment with 20 nM GTX and distinct LRA class compounds [2 nM RMD, 350 nM SAHA, 1 μM CAPE, 2 μM OTX-01, 0.5 μM JQ-1, and 0.2 μM prostratin (A) and 1 μM CAPE and 5 μM BRD-K98645985 (B)] and shown as fold increase in luciferase activity. S indicates compound synergism in latency reversal according to the Bliss independence score. (**C**) Cytotoxicity of GTX alone and combined with indicated LRAs in CD4$^+$ T cells. Unstimulated or αCD3/αCD28-stimulated PBMCs were cotreated as indicated for 72 hours followed by annexin V staining, and cell death (AnnexinV$^+$ CD3$^+$CD4$^+$) was determined by flow cytometry. (**D**) GTX (20 nM) does not alter activation of CD4$^+$ T cells. PBMCs from healthy donors were incubated with the indicated LRAs for 72 hours, either unstimulated or stimulated with αCD3/αCD28 antibodies. Panels depict pooled data showing the frequency of CD25$^+$ cells within CD4$^+$ T cells. (**E**) Absolute, cell-associated (CA) *pol* copy number in CD4$^+$ T cells isolated from five aviremic participants that were treated in vitro with vehicle control (Untr), GTX (20 and 40 nM), or positive control for 24 hours as indicated. Statistical significance was calculated using *t* test (*$P < 0.05$; **$P < 0.005$; ***$P < 0.0005$). ns, not significant. (**F**) Data presented in (D) had been averaged and plotted together. Each symbol represents aviremic participant: green, participant 1; blue, participant 2; white, participant 3; yellow, participant 4; and pink, participant 5. Statistical significance was calculated using unpaired Mann-Whitney test (*$P < 0.05$).

not inhibit CD25 expression (Fig. 3D and fig. S5, A and B) or proliferation of activated CD4$^+$ or CD8$^+$ T cells (fig. S5, C and D).

GTX enhances activity of other LRA class molecules and synergizes strongly with histone deacetylase and BAF inhibitors

To investigate possible synergies, we tested the latency reversal potential of GTX (20 nM) in combination with a panel of known LRAs in the J-Lat A2 and 11.1 models of latency (fig. S6) as well as in ex vivo infected primary CD4$^+$ T cells (Fig. 3, A and B). GTX cotreatment enhanced the latency reversal activity observed after single treatments with all compounds (Fig. 3, A and B). When latent HIV-1–infected primary CD4$^+$ T cells were cotreated with GTX (20 nM) and either the histone deacetylase (HDAC) inhibitor suberoylanilide hydroxamic acid (SAHA) or BAF (BRG1- or BRM-associated factors) inhibitors caffeic acid phenethyl ester (CAPE) [at 1 μM concentration in which it does not inhibit nuclear factor κB (NF-κB)] (*27*) or BRD-K98645985 (*28*), synergistic reversal of HIV-1 latency was observed (Fig. 3, A and B). Cotreatments with BET (bromodomain and extra-terminal proteins) inhibitors JQ-1 and OTX-015, as well

as prostratin, resulted in an additive effect on HIV-1 provirus expression. In the primary $CD4^+$ T cell model of HIV-1 latency, GTX treatment alone showed more potent latency reversal activity than SAHA, CAPE, OTX-015, JQ-1, or romidepsin (RMD) alone at tested noncytotoxic concentrations (Fig. 3, A and B). RMD treatment showed modest latency reversal activity (Fig. 3A) and, consistent with the literature (*13*), significant $CD4^+$ and $CD8^+$ T cell cytotoxicity (Fig. 3C and fig. S4, A and B). With the exception of RMD, we did not observe any negative impact of these cotreatments on viability and proliferation of $CD4^+$ T cells (Fig. 3C and fig. S5C), $CD8^+$ T cells (figs. S4, A and B, and S5D), and other immune subpopulations, including $CD19^+$ B cells, $CD56^+$ NK cells, and $CD14^+$ monocytes (fig. S4C). Moreover, none of the cotreatments altered the activation status of either resting or activated $CD4^+$ and $CD8^+$ T cells (Fig. 3D and fig. S5, A and B). Our observed synergistic effects upon GTX cotreatment with BAF inhibitors and the HDAC inhibitor SAHA suggested that GTX may target a different pathway for HIV-1 latency reversal, as targeting the same pathway with different molecules would more likely result in additive effects. Unlike SAHA, GTX treatment of $CD4^+$ T cells did not result in increased histone acetylation (fig. S7A). Similarly, we excluded that GTX behaves as a protein kinase C (PKC) agonist, as treatment with GTX did not induce T cell activation or the expression of PKC pathway target genes (Fig. 2G and fig. S7B).

GTX reverses HIV-1 latency after ex vivo treatment of $CD4^+$ T cells from all aviremic HIV-1–infected study participants

We next examined the potential of GTX to reverse latency after ex vivo treatment of $CD4^+$ T cells obtained from people living with HIV-1. All five participants enrolled were treated with cART and maintained HIV-1 viremia below 50 copies/ml for at least 2 years. Despite differences in the size of the latent pool, assessed by maximal stimulation of the cells with α-CD3/CD28 beads or PMA/ionomycin, GTX treatment at noncytotoxic 20 and 40 nM concentrations significantly increased the levels of cell-associated HIV-1 *pol* RNA copies (CA-*pol* copies) in $CD4^+$ T cells obtained from aviremic HIV-1^+ participants (Fig. 3, E and F). Notably, the observed GTX effect is systematic, as latency reversal was uniformly observed in cells of all tested participants after 24 hours of stimulation (Fig. 3, E and F). This observed latency reversal at the RNA level is the first step consistent with induction of protein expression, although this is not formally examined here. In addition, we observed no increase in expression of genes related to T cell–specific responses, reactive oxygen species, or apoptosis, previously reported pleiotropic effects of GTX observed at significantly higher concentrations (fig. S7C). These results therefore indicate that GTX treatment at nontoxic concentrations reverses latency without inducing immune cell toxicity or activation and without affecting T cell proliferation, rendering GTX a promising potential candidate for further clinical investigation in context of HIV-1 latency reversal and inclusion in "shock and kill" strategies.

GTX reverses HIV-1 latency via disruption of 7SK snRNP, leading to release of active P-TEFb

To gain insight into the molecular mechanism by which GTX reverses latency, we performed RNA sequencing of primary resting $CD4^+$ T cells isolated from healthy blood donors that were treated for 4 hours with 20 nM GTX. This short incubation time was chosen to focus on primary effects of GTX on the global transcriptome, decreasing the presence and likelihood of secondary transcriptional effects. We observed a very good correlation between treatments of two independent healthy blood donors (Fig. 4A, top). Moreover, less than 700 genes showed an altered differential expression pattern (Fig. 4A, bottom). Small nuclear RNA 7SK was the most decreased (more than ninefold) transcript after GTX treatment in $CD4^+$ T cells from the independent donors (Fig. 4, A and B). 7SK RNA serves as a scaffold for the 7SK snRNP complex that sequesters the P-TEFb and inhibits its activity (*29*–*33*). Among all components of the 7SK snRNP complex and its close interactors, only the 7SK transcript was affected by treatment with GTX (Fig. 4B and fig. S9A). Consistent with our observations after treatment of $CD4^+$ T cells obtained from aviremic participants (fig. S7C), we did not detect significant change in expression of NF-κB, oxidative stress, apoptosis, and T cell effector function-related genes after GTX treatment (figs. S7B and S8), indicating that GTX (20 nM) treatment does not influence these pathways after 4 or 24 hours of stimulation. As P-TEFb is an essential cofactor for Tat-mediated HIV-1 transcription elongation (*34*, *35*), we examined whether GTX treatment affects P-TEFb activity. Phosphorylation of Ser^2 residues within the CTD of RNA Pol II is a prerequisite for activation of transcription elongation and is mediated by the kinase activity of cyclin-dependent kinase 9 (CDK9), a component of P-TEFb (*36*). To examine whether GTX treatment resulted in Ser^2 RNA Pol II phosphorylation, we treated resting $CD4^+$ T cells with GTX, the CDK9 inhibitor flavopiridol (FPD), and PMA or αCD3/αCD28 as positive control (Fig. 4C and fig. S9B). As expected, FPD treatment abrogated RNA Pol II phosphorylation, while PMA stimulation led to strong Ser^2 RNA Pol II phosphorylation. Treatment with GTX caused an increase in phosphorylation of the CDK9 target RNA Pol II Ser^2 in three independent donors tested (Fig. 4, C and D, and fig. S9B). We also examined potential Tat-independent effects of GTX on basal HIV-1 transcription by comparing GTX-induced reactivation in J-Lat A72 cells, which lack Tat, with that in J-Lat A2 cells (fig. S9C). While GTX robustly reactivated transcription in Tat-containing A2 cells, in comparison, A72 cells were not significantly reactivated. These results support a Tat-dependent mechanism of GTX function consistent with a role in enhancing Tat–P-TEFb–mediated HIV-1 transcription.

The fact that short-term GTX treatment enhanced P-TEFb activity in resting $CD4^+$ T cells without cellular activation (Figs. 2G, 3D, and 4C) led us to hypothesize that GTX treatment may cause destabilization of the 7SK snRNP complex, leading to the release of free (active) P-TEFb. Active P-TEFb would then become available for transcription elongation at the latent HIV-1 LTR, a critical step required for HIV-1 latency reversal (*37*–*39*). To test this, we performed glycerol gradient sedimentation experiments after treatment of resting $CD4^+$ T cells with GTX (Fig. 4, E to G, and fig. S9D). GTX treatment (20 nM) of $CD4^+$ T cells for 4 hours resulted in release of free P-TEFb from its inhibitory higher–molecular weight 7SK snRNP complex, as shown by Western blot analysis depicting distribution of the P-TEFb component CDK9 over high– and low–molecular weight fractions (Fig. 4F and fig. S9D). As expected, control treatment of $CD4^+$ T cell lysates with ribonuclease A (RNase A), which digests the 7SK RNA scaffold, resulted in release of free P-TEFb, which eluted at lower–molecular weight fractions (Fig. 4F and fig. S9D). Quantification of free versus 7SK snRNP–sequestered P-TEFb demonstrates a significant GTX-induced release of free P-TEFb from the 7SK snRNP complex in $CD4^+$ T cells from three independent donors (Fig. 4G). CDK9 T-loop phosphorylation at Thr^{186} is critical for the kinase

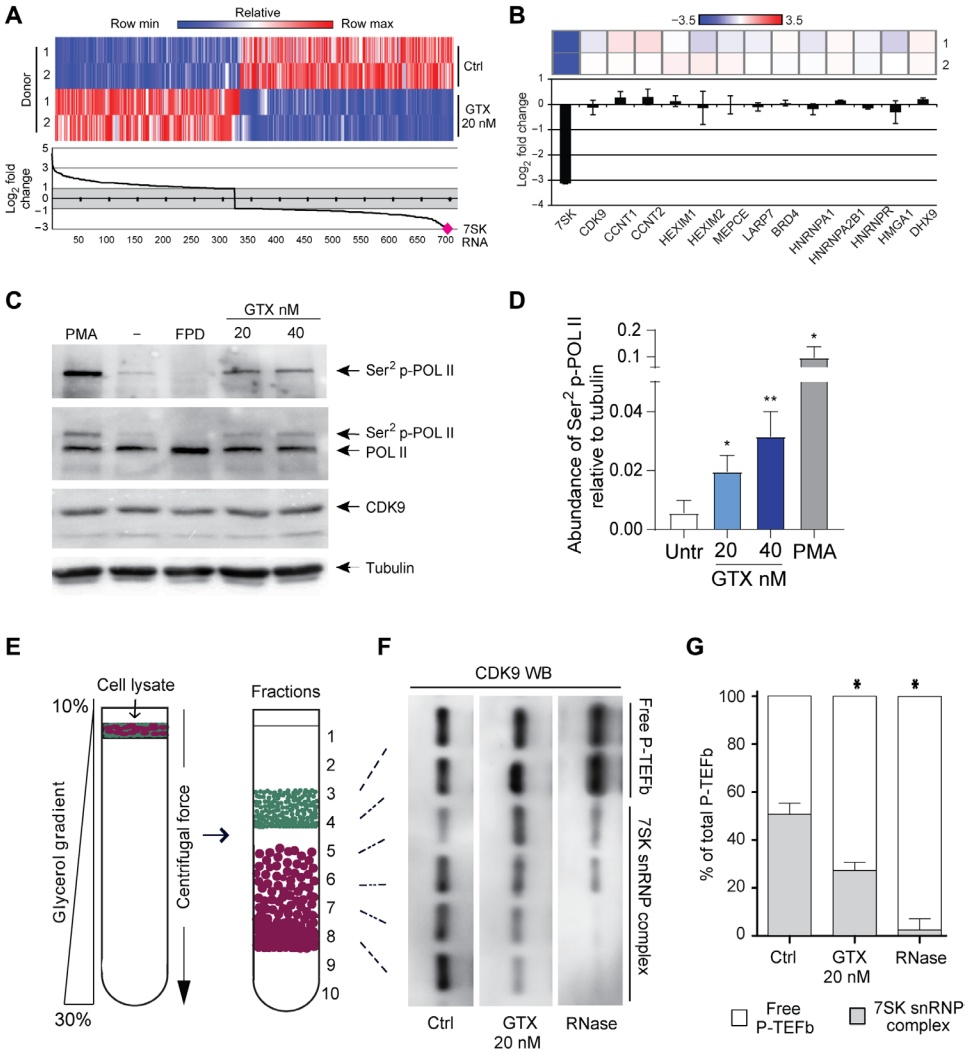

Fig. 4. GTX treatment of resting CD4$^+$ T cells causes decrease in 7SK RNA and activation of P-TEFb activity. (**A**) Heatmap of differentially expressed genes obtained from RNA sequencing analysis of primary CD4$^+$ T cells treated as indicated for 4 hours (top). RNA sequencing indicates 7SK RNA to be the most differentially decreased gene in response to GTX treatment of CD4$^+$ T cells in two independent donors (bottom). (**B**) GTX treatment of primary CD4$^+$ T cells for 4 hours leads to specific depletion of 7SK RNA levels and not mRNA levels of other components of the 7SK snRNP complex. (**C**) Representative Western blot (WB) analysis of CTD Ser^2 phosphorylation of RNA Pol II mediated by CDK9 in primary CD4$^+$ T cells treated for 6 hours with GTX as indicated. PMA was used as a positive control, and FPD was used as a negative control. (**D**) Quantification of bands representing phosphorylated RNA Pol II normalized to tubulin and relative to untreated control from three independent experiments (C; fig. S9C). Statistical significance was calculated using unpaired *t* test (*$P < 0.05$; **$P < 0.01$). (**E** and **F**) GTX treatment causes release of P-TEFb from sequestration within the 7SK snRNP complex. (E) Schematic of glycerol gradient experiments, in which cell lysates (from GTX-treated or untreated cells) are loaded on top of generated glycerol gradients (10 to 30%) and ultracentrifuged, followed by collection of fractions, trichloroacetic acid protein precipitation, and subsequent analysis by SDS–polyacrylamide gel electrophoresis Western blotting. (F) Representative Western blot analysis of glycerol gradient sedimentation of lysates from primary CD4$^+$ T cell, which were treated (6 hours) with GTX (20 nM) or vehicle control as indicated using antibodies specific for the P-TEFb component CDK9. As control, untreated lysates were treated with RNase for 1 hour to digest 7SK RNA and release P-TEFb. (**G**) Quantification of free versus total CDK9 in primary CD4$^+$ T cells treated as indicated, as shown in (F) and fig. S9E, from three independent donors. Statistical significance was calculated using unpaired *t* test (*$P < 0.05$).

activation and its dissociation from the 7SK snRNP (*40*). In resting CD4$^+$ T cells, cyclin T1 levels are low, as are the levels of CDK9 T-loop phosphorylation (*39*). To check whether GTX-induced release of P-TEFb involves increased CDK9 T-loop phosphorylation or increase in cyclin T1 levels, we treated primary CD4$^+$ T cells with increasing concentrations of GTX for 6 hours and used PMA as positive control. At 6 hours after treatment, at a time point in which we observe phosphorylation of RNA Pol II CTD (Fig. 4, C and D), GTX treatment does not cause phosphorylation of CDK9 at Thr^{186}, nor does it lead to increased cyclin T1 levels (fig. S9, E and F), demonstrating that these mechanisms are not involved in GTX-induced latency reversal at this early time point.

To understand better which component of the 7SK snRNP complex may be targeted by GTX, we performed in silico docking experiments using two independent software packages, Chimera and Achilles. We modeled GTX against all essential components of the complex separately, as complete crystal structure of 7SK snRNP is not yet available. Notably, we observed preferential binding of GTX

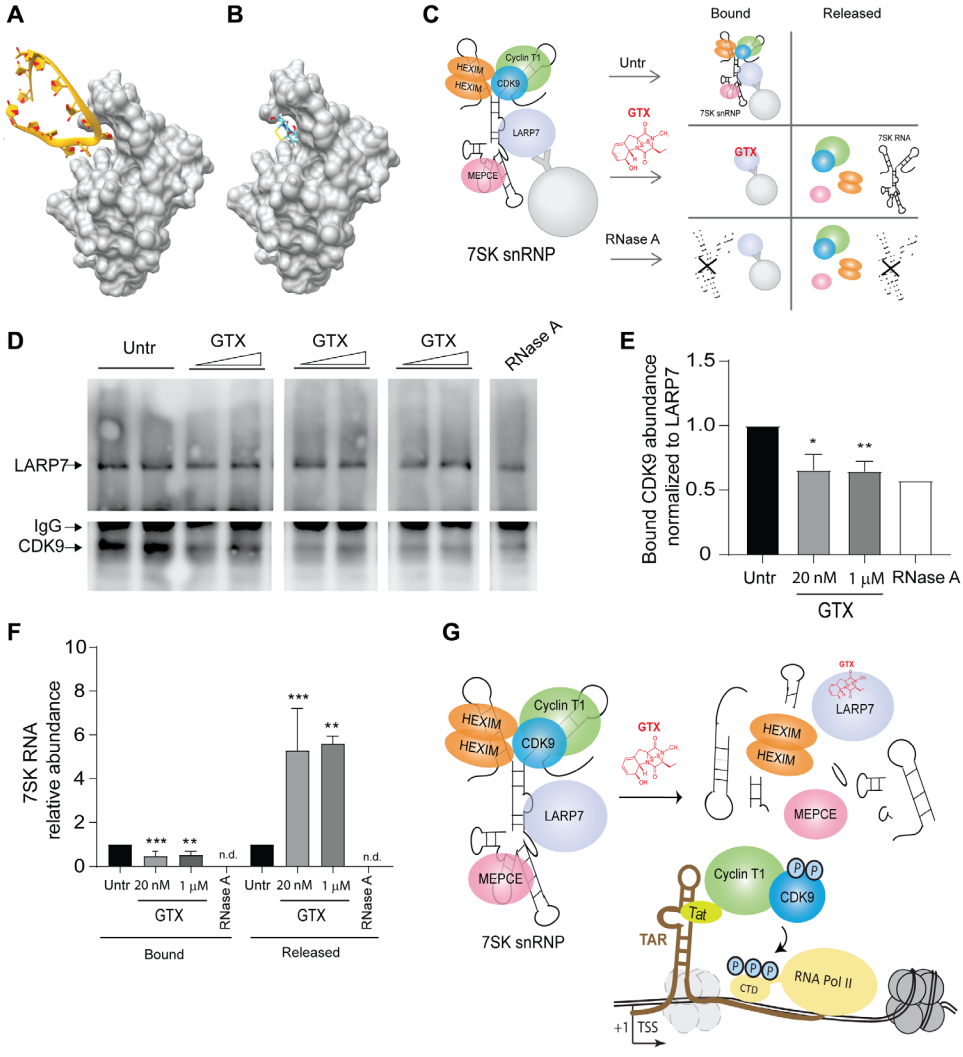

Fig. 5. GTX disrupts 7SK snRNP, causing release of P-TEFb and enhanced HIV-1 transcription. (**A**) Crystal structure of human LARP7 CTD in complex with 7SK RNA SL4 (Protein Data Bank ID code 6D12). LARP7 is shown in space-filling representation (gray) with bound RNA as yellow cartoon representation with bases indicated as flat rings (oxygen in red). (**B**) Proposed binding mode of GTX into the deep pocket on the surface of LARP7 as predicted by Chimera's AutoDock Vina function and the Achilles Blind Docking server. Color code for GTX: carbon (turquoise), oxygen (red), sulfur (yellow), hydrogen (white), and nitrogen (blue). (**C**) Schematic representation of the 7SK snRNP coimmunoprecipitation CDK9 release experiment. (**D**) 7SK snRNP complex is immunoprecipitated using beads coated with anti-LARP7. Beads are divided and left either untreated or treated with GTX 20 nM or 1 μM or RNase A as indicated. Bead-bound fractions are separated and subjected to Western blot analysis to detect presence of LARP7 and CDK9. IgG, immunoglobulin G. (**E**) Quantification of CDK9 abundance normalized to immunoprecipitated LARP7 and relative to untreated control ($n = 3$). Statistical significance was calculated using unpaired t test (*$P < 0.05$; **$P < 0.01$). (**F**) 7SK RNA release assay from immunoprecipitated 7SK snRNP complex, as represented in (C). Bound and released fractions are subjected to reverse transcription quantitative polymerase chain reaction to quantitate the levels of bead-bound and released 7SK RNA in reaction supernatant. Input 7SK RNA (prereaction beads) was used for normalization. Statistical significance was calculated with unpaired t test ($n = 3$, **$P < 0.01$; ***$P < 0.001$; n.d., not detected). (**G**) Proposed model for GTX-mediated transcription activation of the latent HIV-1 LTR via degradation of 7SK RNA and release of CDK9 from the 7SK snRNP complex. Free P-TEFb is then recruited to the HIV-1 Tat-TAR axis, leading to phosphorylation of RNA Pol II at Ser^2 and subsequent stimulation of transcription elongation.

into the hydrophobic pocket of LARP7, which, in physiological conditions, is responsible for binding stem loop 4 (SL4) of the 7SK RNA (Fig. 5, A and B, and fig. S10). LARP7 is a critical component, responsible for stabilization of the 7SK snRNP complex, as its depletion has been shown to lead to decreased levels of 7SK RNA with concomitant increase in free P-TEFb levels (*41*). To test whether GTX interferes with LARP7-7SK RNA binding, we performed a 7SK RNA release assay (Fig. 5, C to F). 75K snRNP complex was immunoprecipitated and immobilized on protein G beads using a LARP7 antibody. 7SK snRNP–bound beads were then either left untreated or treated with GTX or RNase A as indicated, and the presence of LARP7-bound CDK9 was examined by Western blot analysis of the bead-bound fraction (Fig. 5, D and E). As expected, RNase A treatment resulted in direct disruption of the 75K snRNP complex as measured by release of the CDK9 component into the supernatant and its separation from the bead-bound LARP7 component (Fig. 5, D and E). GTX treatment also resulted in release of CDK9 as observed in relative decrease in LARP7-bound

CDK9 as determined by Western blot analysis (Fig. 5, D and E). In agreement, treatment with GTX resulted in a concomitant significant decrease in abundance of scaffold 7SK RNA from the bead-bound 7SK snRNP fraction as well as an approximately sixfold increase in levels of 7SK RNA in the released fraction (Fig. 5F).

Our experimental data, together with this modeling exercise and previously published data, are consistent with a model in which GTX interferes with the binding of SL4 of 7SK RNA into the hydrophobic pocket of LARP7, which results in destabilization of the complex and subsequent release of P-TEFb and 7SK RNA (Fig. 5, D to G). In resting $CD4^+$ T cells, 7SK RNA is then degraded and free P-TEFb made available for recruitment to the paused RNA Pol II at the latent HIV LTR by the Tat-TAR (trans-activation response element) axis. CDK9 then phosphorylates CTD of RNA Pol II, leading to activation of proviral transcription elongation (Fig. 5G).

DISCUSSION

Distinct classes of LRAs have been shown to target different subpopulations of proviruses (*9*, *19*, *42*, *43*). Thus far, none of the clinically tested LRAs have been able to induce strong viral expression or to significantly deplete the latent reservoir in patients, pointing to potential limitations of single treatments (*6*, *7*). The heterogeneous nature of latent HIV integrations and the complex molecular mechanisms that contribute to maintaining HIV latency, together with individual genetic variability, dictate that a cocktail of stimulatory compounds targeting distinct cellular and HIV gene regulatory pathways would be most effective to activate the latent reservoir in HIV-1–infected patients (*19*). Preclinical studies demonstrate that combination treatments can result in synergism and lead to stronger HIV-1 latency reversal (*11*, *19*, *27*, *28*, *44*–*48*). Here, we found that GTX, a molecule that targets the HIV-1 transcription elongation step, strongly synergized with LRAs that derepress chromatin structure, namely, BAF and HDAC inhibitors, which respectively target complexes that position the latent LTR chromatin in a repressive configuration (*49*) or deacetylate histones compacting LTR chromatin. Cotreatment of primary latently infected $CD4^+$ T cells with GTX and BET inhibitors resulted in additive and not synergistic increase in HIV transcription. This observation is consistent with the fact that these compounds target the same mechanistic step: transcription elongation at the HIV-1 LTR. Our data highlight the attractiveness of simultaneous pharmacological targeting of mechanistically distinct steps in HIV-1 transcription regulation, namely, at the level of chromatin structure, transcription factor–induced activation and transcription elongation. We postulate that more robust latency reversal will be observed when compounds targeting these three mechanistic steps are combined, and further optimized by interventions that address blocks occurring posttranscriptionally, at the polyadenylation and splicing stages, which may hinder translation of HIV-1 genes (*38*). In addition, consistent with the importance of targeting transcription elongation, shown recently to be a major rate-limiting step in HIV-1 latency reversal in patient $CD4^+$ T cells (*38*), ex vivo GTX treatment of $CD4^+$ T cells obtained from cART-suppressed aviremic HIV-1–infected patients demonstrated significant increase in levels of cell-associated HIV-1 RNA in all patients examined.

GTX causes disruption of the 7SK snRNP complex with subsequent release of active P-TEFb by directly targeting LARP7. Other molecules including HMBA (hexamethylene bisacetamide) (*50*) and DRB (5,6-Dichloro-1-β-d ribofuranosylbenzimidazole) and actinomycin D (*30*, *32*) have also previously been shown to cause 7SK snRNP disruption although through indirect mechanisms. Given the significance of P-TEFb in HIV transcription elongation and the current lack of available molecules able to mediate its release from the inhibitory 7SK snRNP complex, GTX may be a promising candidate not only in the context of HIV-1 latency reversal but also in other diseases in which P-TEFb plays a prominent regulatory role (*51*). Our modeling exercises provide insight toward a mechanism where GTX competes with 7SK RNA for the hydrophobic pocket of LARP7, causing destabilization and disassembly of the 7SK snRNP complex, leading to the release of P-TEFb and subsequent degradation of the 7SK RNA scaffold as observed in our experiments (Figs. 4 and 5 and figs. S9 and S10). LARP7 has been shown to be a critical scaffold required for the stability of the 7SK snRNP complex; consistent with our observations, RNA interference–mediated depletion of LARP7 resulted in elevated levels of free P-TEFb and increased Tat-mediated HIV-1 expression, concomitant with degradation of 7SK RNA (*41*).

Thus far, GTX has been regarded as a toxin and a virulence factor of *Aspergillus* spp. fungi, shown to function as an immunosuppressant that inhibits phagocytosis, blocks NF-κB signaling and cytokine production, and induces reactive oxygen species formation (*22*, *24*, *25*, *52*–*55*). These properties are ascribed to the molecule's unusual disulfide bridge, which may mediate the activity of GTX by cycling between a reduced and oxidized state (*25*). However, it is important to note that all of the above-mentioned effects of GTX were observed at high concentrations in the 100 nM to 5 μM range, concentrations at which we also observed significant toxicity and cell death (Fig. 2 and figs. S3, S4, and S6). Serum concentrations of GTX reported in patients with aspergillosis are found to be between 200 nM and 2.4 μM (*56*), more than 10 to 100 orders of magnitude higher than concentrations that we have shown to effectively reverse HIV-1 latency in primary T cells and cells of cART-suppressed HIV-1–infected participants (Figs. 3 and 4). Together, these observations suggest that lower GTX concentrations in the 20 nM range, at which effective HIV-1 latency reversal is observed in primary $CD4^+$ T cells without associated toxicity, global T cell activation, or interference with capacity for $CD8^+$ T cells activation, will be physiologically achievable in a therapeutic context. Our data therefore support the potential of GTX for inclusion in combination latency reversal therapeutic approaches in a safe concentration range. Last, our data underlie the power of coupling a screen of fungal extrolites, which comprise a largely unexplored plethora of bioactive chemical entities, with bioassays and state-of-the-art fractionation and MS/NMR as a strategy to identify and characterize novel compounds with therapeutic potential.

MATERIALS AND METHODS

Cells and culture conditions

Jurkat latent (J-Lat) cell lines A2 and 11.1 were cultured in RPMI 1640 media supplemented with 10% fetal bovine serum (FBS) and penicillin-streptomycin (100 μg/ml) at 37°C in a humidified 95% air–5% CO_2 incubator. Primary $CD4^+$ T cells were cultured in RPMI 1640 media supplemented with 7% FBS and penicillin-streptomycin (100 μg/ml) at 37°C in a humidified 95% air–5% CO_2 incubator.

Preparation of fungal supernatants

We screened 115 species of filamentous fungi (table S1 and fig. S1A). The species belonged to 28 orders (43 families) of the fungal kingdom.

The majority were of ascomycetous affinity including ascomycetous yeasts (Saccharomycetales: 4 species), 12 were of basidiomycetous affinity including 3 basidiomycetous yeasts (Trichosporonales and Tremellales) and 3 species of lower fungi (Mucorales) (*57*). Rationale for choice was the expected production of a wide array of metabolites, which are known to be more pronounced in fungi living in habitats with environmental stress or microbial competition. Particularly versatile nutrient scavengers in Eurotiales and Hypocreales are established metabolite and toxin producers. Onygenales are cellulose and keratin degraders and contain a large cluster of mammal pathogens with alternating environmental life cycles. Members of Capnodiales are saprobes in environments with stressful microclimates such as rock, glass, and indoor. Identity of all strains was verified by recombinant DNA internal transcribed spacer and partial nucLSU (D1/D2 of large subunit) sequencing. Strains were derived from lyophilized storage in the reference collection of the Centraalbureau voor Schimmelcultures (housed at the Westerdijk Fungal Biodiversity Institute, Utrecht, The Netherlands). After opening, contents of vials were taken up in 1 ml of malt peptone and distributed on Malt Extract Agar (MEA; Oxoid) culture plates. Strains were maintained on MEA slants and subcultured regularly until use. Mycelial fragments of 1-week-old colonies grown on MEA at 25°C were used as inocula for 500-ml flasks containing 150 ml of RPMI 1640 (with glutamine), shaken at 180 rpm and incubated at 25°C for 7 days, with one negative control. Flasks were checked daily until biomass reached one-third to one-fourth of the volume and then harvested by centrifugation at 14,000*g* and filtered using 0.2-μm metal filters. Supernatants were transferred to Falcon tubes and used for latency screens. One strain per genus was used in a first round; additional isolates, some of which were close relatives and others located at larger phylogenetic distance, were tested in case of positive response. Positive tests of strain *A. fumigatus* CBS 113.26 was thus followed by *A. fumigatus* CBS 154.89, CBS 117884, and CBS 100074, *Aspergillus lentulus* CBS 117884, and *A. flavus* CBS 625.66.

Fractionation and MS characterization of active components

Complex fungal supernatants (3.3 ml) were twice extracted with ethylacetate (3 ml) in glass tubes (5-min vortex) and centrifuged at 3000 rpm. Water phase was discarded and organic extract dried in a vacuum concentrator. Lipids were removed by consequent hexane/water extraction [50/50 (v/v), 4-ml total volume], and aqueous phase was collected and dried. The dried material was reconstituted in 50% methanol (MeOH) and such a solution loaded onto HLB, MCX (Mixed-mode, strong Cation-eXchange), and MAX (Mixed-mode, strong Anion-eXchange) cartridges (Fig. 2, A and B) obtained from Waters Corporation (Prague, Czech Republic). The adsorbed compounds were desalted and stepwise eluted with increasing (5, 45, and 95%) organic solvent (MeOH) gradient (1% HCOOH), providing A, B, and C sample variants, respectively (Fig. 2B). HLB was based on *N*-vinylpyrrolidone–divinylbenzene copolymer and provided 5 fractions. MCX was a cation-exchange sorbent that represented the HLB material modified with SO_3H^- groups (6 fractions). The best performance was provided by anion-exchange MAX cartridge, providing 7 fractions. After each round of fractionation, all samples were tested in J-Lat/S-Lat latency models, followed by quantitation GFP/luciferase expression and identification of fraction-retaining activating component. As expected, originally less active fractions have become positive, as the active components became populated during the enrichment process. The same phenomenon was observed when working with less or more active *Aspergillus* strains (fig. S2B). The most active 7B/7C fractions were further fractioned on HLB cartridge (11 samples) and components dereplicated by CycloBranch software (*20*). Compound matching against the annotated database of *Aspergillus* secondary metabolites has revealed a set of candidate compounds further selected for latency reversal testing. GTX was present in active fractions (Fig. 2B and fig. S2B). Detailed examination of commercial (GTX, Cayman and ApexBio) and natural GTXs was performed by high-performance liquid chromatography and Fourier transform ion cyclotron resonance (FTICR) MS. A solariX XR 12T FTICR instrument (Bruker Daltonics, Billerica, USA) was operated in a positive ion mode with electrospray ionization. Separation of GTX components was performed on an Acquity UPLC HSS T3 analytical column (Waters, Prague, Czech Republic) with 1.0 mm by 150 mm dimensions and 1.8-μm particle size. The analysis was carried out at 30°C and a 30 μl/min flow rate with the following A/B gradient: 0 min, 30% B; 30 min, 95% B; 40 min, 95% B; 50 min, 30% B; 60 min, 30% B. The gradient components A and B were represented by 0.1% formic acid in water or acetonitrile (ACN), respectively. One-minute time windows around S2 and S3/S4 GTXs were used for fraction isolation. The preparative chromatography was performed both with commercial GTX and with *A. fumigatus* 100074 strain.

Flow cytometry and annexin V staining

GFP expression of cell lines J-Lat A2 and 11.1 and phenotype of spin-infected primary $CD4^+$ T cells at the moment of reactivation were analyzed by fluorescence-activated cell sorting (FACS) as described previously (*27*). For annexin V staining, 10^6 cells were washed with phosphate-buffered saline (PBS) supplemented with 3% FBS and 2.5 mM $CaCl_2$ and stained with annexin V–PE (phycoerythrin) (Becton and Dickinson) for 20 min at 4°C in the dark in the presence of 2.5 mM $CaCl_2$. Stained cells were washed with PBS/FBS/$CaCl_2$, fixed with 1% formaldehyde, and analyzed by FACS.

Primary $CD4^+$ T cell isolation and infection

Primary $CD4^+$ T cells were isolated from buffy coats from healthy donors by Ficoll gradient (GE Healthcare) followed by negative selection with RosetteSep Human $CD4^+$ T Cell Enrichment Cocktail (STEMCELL Technologies). Isolated cells were left overnight for recovery and used for spin infection according to Lassen and Greene method as described previously (*27*, *58*). Briefly, $CD4^+$ T cells were infected with the pNL4.3.Luc.R-E- virus by spinoculation (120 min at 1200*g*) and cultured for 3 days in RPMI 1640, 10% FBS, and penicillin-streptomycin (100 μg/ml) in the presence of saquinavir mesylate (5 μM). Three days after infection, cells were treated as indicated in the presence of raltegravir (30 μM). Cells were harvested 24 hours after treatment, and luciferase activity was measured using the Luciferase Assay System (Promega, Leiden, The Netherlands). Infections were performed using pseudotyped particles obtained by cotransfecting HXB2-Env with pNL4.3.Luc.R-E- plasmid into human embryonic kidney 293T cells using polyethylenimine 48 and 72 hours after transfection, and supernatants containing pseudotyped virus were collected, filtered with a 0.45-μm filter, and stored at −80°C. Molecular clones pNL4.3.Luc.R-E- and HIV-1 HXB2-Env and antiretroviral drugs saquinavir mesylate and raltegravir were provided by the Centre for AIDS Reagents, National Institute for Biological Standards and Control. HIV-1 molecular

clone pNL4.3.Luc.R-E- and HIV-1 HXB2-Env expression vectors were donated by N. Landau and by K. Page and D. Littman, respectively.

HIV-1 latency reversal in primary CD4$^+$ T cells isolated from aviremic patients

Primary CD4$^+$ T cells were isolated as described previously (*27*). Three million CD4$^+$ T cells were plated in triplicate at a cell density of 10^6/ml and treated as indicated. After 24 hours, cells were lysed, and total RNA was isolated as described below. Written informed consent was obtained from all patients involved in the study. The study was conducted in accordance with ethical principles of the Declaration of Helsinki. The study protocol and any amendment were approved by The Netherlands Medical Ethics Committee (MEC-2012-583).

Total RNA isolation and quantitative reverse transcription polymerase chain reaction

Cells were lysed in TRI reagent, and RNA was isolated with the Total RNA Zol-Out kit (A&A Biotechnology); complementary DNA (cDNA) synthesis and quantitative polymerase chain reaction (qPCR) was performed as described previously (*27*). Gene expression was calculated using the $2^{-\Delta\Delta Ct}$ method (*59*), and expression of glyceraldehyde phosphate dehydrogenase (GAPDH) was used for normalization. Absolute quantification of cell-associated *pol* RNA was performed as described previously (*27*). Briefly, qPCR was performed in a final volume of 25 μl using 4 μl of cDNA, 2.5 μl of 10× PCR buffer (Life Technologies), 1.75 μl of 50 mM $MgCl_2$ (Life Technologies), 1 μl of 10 mM deoxynucleotide triphosphates (Life Technologies), 0.125 μl of 100 μM Pol forward primer (HXB2 genome 4901 → 4924), 0.125 of 100 μM Pol reverse primer (HXB2 genome 5060 → 5040), 0.075 μl of 50 μM of Pol probe, and 0.2 μl of Platinum Taq polymerase (Life Technologies). The lower limit of detection of this method was of 20 copies of HIV-1 RNA in1 μg of total RNA. The absolute number of pol copies in PCR was calculated using standard curves ranging from 7 to 480 copies of a plasmid containing the full-length HIV-1 genome (pNL4.3.Luc.R-E-). The amount of HIV-1 cell-associated RNA was expressed as the number of copies per microgram of input RNA in reverse transcription. Preparations of cell-associated RNA were tested for potential contamination with HIV-1 DNA and/or host DNA by performing the PCR amplification in the presence and absence of reverse transcriptase.

Primers used for reverse transcription (RT)–qPCR were as follows: pol forward, 5′GGTTTATTACAGGGACAGCAGAGA3′ and pol reverse, 5′ACCTGCCATCTGTTTTCCATA3′; pol probe, [6FAM] AAA ATT CGG TTA AGG CCA GGG GGA AAG AA[BHQ1]; tumor necrosis factor–α (TNFα) forward, 5′TAGGCTGTTCCCATGTAGCC3′ and TNFα reverse, 5′CAGAGGCTCAGCAATGAGTG3′; interleukin-2 (IL-2) forward, 5′ACCTCAACTCCTGCCACAAT3′ and IL-2 reverse, 5′GCACTTCCTCCAGAGGTTTG3′; IFNγ forward, 5′ATAATGCAGAGCCAAATTGTCTCC3′ and IFNγ reverse, 5′ATGTCTTCCTTGATGGTCTCCAC3′; CD25 forward, 5′ATCAGTGCGTCCAGGGATAC3′ and CD25 reverse, 5′GACGAGGCAGGAAGTCTCAC3′; BAK1 (Brassinosteroid Insensitive 1-associated receptor kinase 1) forward, 5′GGTTTTCCGCAGCTACGTTTTT3′ and BAK1 reverse, 5′GCAGAGGTAAGGTGACCATCTC3′; BAX (BCL-2-associated X protein) forward, 5′CCCGAGAGGTCTTTTTCCGAG3′ and BAX reverse, 5′CCAGCCCATGATGGTTCTGAT3′; BCL2 (B-Cell lymphoma 2 protein) forward, 5′GGTGGGGTCATGTGTGTGG3′ and BCL2 reverse, 5′CGGTTCAGGTACTCAGTCATCC3′; CASP-3 (Caspase-3 protein) forward, 5′CATGGAAGCGAATCAATGGACT3′ and CASP-3 reverse, 5′CTGTACCAGACCGAGATGTCA3′; AKT1 (RAC-alpha serine/threonine-protein kinase) forward, 5′AGCGACGTGGCTATTGTGAAG3′ and AKT1 reverse, 5′GCCATCATTCTTGAGGAGGAAGT3′; NRF2 (NFE2-related factor 2 protein) forward, 5′TTCCCGGTCACATCGAGAG3′ and NRF2 reverse, 5′TCCTGTTGCATACCGTCTAAATC3′; FOXO3a forward, 5′CGGACAAACGGCTCACTCT3′ and FOXO3a reverse, 5′GGACCCGCATGAATCGACTAT3′; KEAP1 (Kelch-like ECH-associated protein 1) forward, 5′GCAATGAACACCATCCGAAGC3′ and KEAP1 reverse, 5′ACCATCATAGCCTCCAAGGAC3′; CYCT1 (Cyclin T 1 protein) forward, 5′GGCGTGGACCCAGATAAAG3′ and CYCT1 reverse, 5′CTGTGTGAAGGACTGAATCAT3′; CDK9 forward, 5′ATGGCAAAGCAGTACGACTCG3′ and CDK9 reverse, 5′GCAAGGCTGTAATGGGGAAC3′; GAPDH forward, 5′CAAGAAGGTGGTGAAGCAG3′ and GAPDH reverse, 5′GCCAAATTCGTTGTCATACC3′; and B2M forward, 5′ATGAGTATGCCTGCCGTGTG3′ and B2M reverse, 5′CCAAATGCGGCATCTTCAAAC3′.

Glycerol gradient sedimentation

Glycerol gradients were prepared as described previously (*50*). Briefly, around 40 × 10^6 primary CD4$^+$ T cells isolated from healthy donors were either untreated or treated with GTX (20 nM) for 4 hours for RNase A treatment. Cells were lysed for 30 min in buffer A supplemented either with RNasin (100 U/ml; Promega) for untreated and GTX conditions or with RNase A (100 μg/ml). RNase-supplemented lysates were incubated for 10 min at room temperature to ensure efficient degradation of RNA. Lysates were fractionated by centrifugation in a SW41 Ti rotor at 38,000 rpm for 20 hours. Fractions (1 ml) were collected in 2-ml tubes and subjected to trichloroacetic acid (TCA) precipitation of proteins as described previously (*60*). Briefly, to each 1 ml of fraction, 110 μl of ice-cold 100% TCA was added and incubated on ice for 10 min. Then, 500 μl of ice-cold 10% TCA was added to each sample and incubated on ice for 20 min, followed by centrifugation at 20,000*g* for 30 min. Supernatants were carefully removed, and precipitates were gently washed with 500 μl of ice-cold acetone followed by centrifugation at 20,000*g* for 10 min. Supernatants were gently removed and dried at room temperature for about 10 min. Protein precipitates were then resuspended in 50 μl of Laemmli loading buffer and subjected to 10% SDS–polyacrylamide gel electrophoresis (SDS-PAGE) separation and detection of CDK9 (C-20, sc-484, Santa Cruz Biotechnology).

RNA Pol II and CDK9 T-loop phosphorylation

For RNA Pol II phosphorylation, 10 million primary CD4$^+$ T cells were either untreated or treated with GTX, OTX-015 (1 μM), FPD (500 nM), PMA (10 nM), or αCD3/CD28 beads (cell:bead ratio of 1:1) for 6 hours. For CDK9 phosphorylation, 5 million primary CD4$^+$ T cells were either untreated or treated with GTX (20 and 40 nm) or PMA (10 nM) for 6 hours. Four million cells were lysed for 30 min on ice with immunoprecipitation buffer [25 mM Hepes (pH 7.9), 150 mM KCl, 1 mM EDTA, 5 mM $MgCl_2$, 5% glycerol, 1% NP-40, 0.5 mM dithiothreitol (DTT), PhosSTOP phosphatase inhibitor (Sigma-Aldrich), and a cOmplete protease inhibitor cocktail (Sigma-Aldrich)] and subjected to Western blot analysis using the following antibodies: total RNA Pol II (N-20, sc-899, Santa Cruz Biotechnology), phospho-Ser^2 RNA Pol II (H5, ab-24758, Abcam), CDK9 (C-20, sc-484,

Santa Cruz Biotechnology) (Fig. 4C and fig. S9B), total CDK9 (D7, sc-13130, Santa Cruz Biotechnology) (fig. S9E), cyclinT1 (H-245, sc-10750, Santa Cruz Biotechnology), α-tubulin (ab6160, Abcam), and phospho-CDK9 Thr^{186} (#2549, Cell Signaling Technology).

7SK snRNP complex immunoprecipitation and 7SK RNA / CDK9 release assay

Fifty million Jurkat cells were lysed in 5 ml of immunoprecipitation buffer [1% NP-40, 25 mM tris (pH 7.4), 150 mM NaCl, 1 mM EDTA, 5% glycerol, and EDTA-free protease inhibitor cocktail (1 U/ml; Roche)] for 30 min on ice and centrifuged for 10 min at 14,000 rpm. Protein G Sepharose beads (200 μl) were washed two times with lysis buffer. Lysates were incubated with beads and 2 μg of antibody against human LARP7 (A303-723A, Bethyl Laboratories) at 4°C overnight. Next day, the beads were washed two times with lysis buffer, resuspended in 400 μl of lysis buffer containing 1 mM DTT, and divided in four reactions of 100 μl each. The presence of DTT is critical to the activity of GTX in agreement with its lability and known unusual disulfide bridge. Aliquotes were left untreated or treated with GTX for 1 hour or with RNase A for 15 min at room temperature. Next, supernatant was discarded, and beads were washed twice with lysis buffer. Beads were resuspended in 100 μl of Laemmli loading buffer and subjected to 12% SDS-PAGE separation and detection of CDK9 (sc-484, Santa Cruz Biotechnology) and LARP7 by Western blot. Ten microliters of beads suspension before and after treatment and 10 μl of supernatant after treatment were taken and resuspended in TRI reagent (Sigma) for subsequent RNA isolation (Total RNA Zol-Out kit, A&A Biotechnology). cDNA was synthetized using 10 μl of RNA solution as described above and diluted 560 times for quantitative RT-PCR. 7SK RNA was amplified using specific primers described elsewhere (*61*). qPCR was performed as described above. Values were normalized to the input RNA (post-treatment bead suspension).

Histone acetylation

Ten million primary CD4$^+$ T cells were treated with GTX concentration gradient, SAHA, or left untreated for 4 hours and then washed twice in PBS. Cells were lysed for 10 min at 4°C in TBE (Tris-borate-EDTA) buffer [PBS, 0.5% Triton X-100 (v/v), 2 mM phenylmethylsulfonyl fluoride, and 0.02% (w/v) NaN_3] at a density of 10^7 cells per 1 ml of the buffer. Samples were centrifuged at 425*g* for 10 min at 4°C. Supernatants were discarded, and cell pellets were washed in half the volume of TEB buffer used for lysis and centrifuged as before. Supernatants were discarded, and pellets were resuspended in 0.2 N HCl at a density of 4×10^7 cells/ml. Histones were extracted overnight at 4°C and then centrifuged at 425*g* for 10 min at 4°C. Supernatants were collected, protein concentration was determined by Bradford assay, and samples were subjected to SDS-PAGE Western blot. The following antibodies were used in Western blot analysis: anti–acetyl-histone H4 (06-598, Millipore) and anti-histone H2B (ab52484, Abcam).

RNA sequencing and data analysis

Ten million primary CD4$^+$ T cells were stimulated with 20 nM GTX or left unstimulated for 4 hours. Experiment was performed in duplicate on cells isolated from two buffy coats from healthy donors as described above. RNA was isolated as described above. cDNA libraries were generated using the Illumina TruSeq Stranded mRNA Library Prep kit (Illumina). The resulting DNA libraries were sequenced according to the Illumina TruSeq Rapid v2 protocol on an Illumina HiSeq 2500 sequencer. Reads were generated of 50 base pairs in length. Reads were mapped against the GRCh38 human reference using HiSat2 (version 2.0.4). We calculated gene expression values using htseq-count (version 0.6.1) using Ensembl transcript annotation. Heatmaps were generated using MORPHEUS (https://software.broadinstitute.org/morpheus/index.html).

Toxicity assay

PBMCs were isolated by density gradient centrifugation (Ficoll-Hypaque, GE Healthcare Life Sciences) from buffy coats from healthy donors (Sanquin, Amsterdam) and either used immediately or frozen in freezing media [90% FBS/10% dimethyl sulfoxide (DMSO] and stored short term at −80°C. For cytotoxicity testing, cells were cultivated in culture media RPMI 1640 (Life Technologies) supplemented with 10% FBS, 2 mM L-glutamine, penicillin (100 U/ml), and streptomycin-sulfate (100 g/ml) at a concentration of 1×10^6 cells/ml in 24-well plates (Thermo Scientific) that were either uncoated (unstimulated cells) or coated with anti-human CD3 (1 μg/ml; clone UCHT1, no azide/low endotoxin, BD Biosciences) and anti-CD28 (10 μg/ml; clone CD28.2, no azide/low endotoxin, BD Biosciences) monoclonal antibodies (stimulated cells). PMA/ionomycin was added at 50 ng/ml and 1 μg/ml, respectively, and cells were exposed for 16 hours. The following LRAs were added at the concentrations indicated in figures: GTX (ApexBio), SAHA-Vorinostat (Selleck Chemicals), CAPE (MP Biomedicals), and RMD (Sigma-Aldrich). LRAs at indicated concentrations were added to the cultures, and cells were continuously exposed for 72 hours. Since GTX was reconstituted in ACN and all other LRAs in DMSO, both solvents were added to the DMSO/ACN control culture (ACN, 1:10000; DMSO, 1:2500) to control for the effect that these solvents may have on cell viability.

Flow cytometry for cytotoxicity assay

To examine the effects the LRAs have on immune cell subpopulations, cell viability, activation, and proliferation were analyzed by flow cytometry. To determine the cytotoxic effect of the LRAs on cells, AnnexinV staining was used to define apoptotic and dead cells. Surface antigens were detected by incubating 0.8 to 1.0×10^6 cells with predetermined optimal concentrations of monoclonal antibody mixes in FACS wash [FW; Hank's Balanced Salt Solution (Life Technologies), 3% FBS (Life Technologies), 0.02% NaN_3, and 2.5 mM $CaCl_2$] for 20 min at 4°C, washed one time with FW, and fixed with 1% paraformaldehyde. To determine proliferation, cells were stained with 0.07 μM CellTrace Far Red Cell Proliferation dye according to the manufacturer's protocol (Thermo Fisher Scientific) before cultivating for 72 hours with either unstimulated or stimulated conditions in the presence of LRA. Upon cell division, the proliferation dye intensity decreases in daughter cells, and this was measured by flow cytometry. The following directly conjugated monoclonal anti-human antibodies were used to analyze CD8$^+$ T cells (CD3$^+$CD8$^+$), CD4$^+$ T cells (CD3$^+$CD4$^+$), B cells (CD3$^-$CD19$^+$), monocytes (CD14$^+$), and NK cells (CD3$^-$CD56$^+$): CD3-BV421 (clone UCHT1), CD4-BV650 (SK3), CD8-BV786 (RPA-T8), CD14-PE-Cy7 (61D3, eBioscience), CD19-PerCP-Cy5.5 (HIB19, eBioscience), CD56-PE-Cy5.5 (CMSSB, eBioscience), annexin V–PE, and CD25$^-$ Super Bright 600 (BC96, eBioscience). All antibodies were purchased from BD Biosciences unless otherwise indicated. Between 2×10^5 and 4×10^5 events were collected per sample within 24 hours after staining on a LSRFortessa (BD Biosciences, 4 lasers, 18 parameters) and analyzed using FlowJo

software (version 9.7.4, Tree Star). Data are represented as frequency within a defined population. Treatment-specific cell cytotoxicity was calculated using the following formula: [(% drug-induced cell death − % cell death in DMSO/ACN only)/(100 − % cell death in DMSO/ACN only)]*100.

Molecular docking

Molecular docking was used to predict the most likely binding mode of GTX to LARP7 CTD. The crystal structure of human LARP7 CTD in complex with 7SK RNA SL4 [Protein Data Bank (PDB) ID code 6D12] was optimized using PDB-REDO (*62*) and used as a template to define the receptor for the docking simulation. The resulting pdb file was manually adapted for input into the docking procedure by elimination of protein chain B and RNA domain C and replacement of selenium atoms (present as selenomethionin, incorporated for phasing purposes) (*63*) by sulfur. GTX ligand structure was built and energy minimized using the program Chimera (*64*). Molecular docking of GTX to LARP7 CTD was performed using the Achilles Blind Docking server (https://bio-hpc.ucam.edu/achilles/) and Chimera's AutoDock Vina function (*65*). The resulting solutions were ranked on the basis of the highest binding affinity (or lowest binding energy). Figures were created using PyMol software (*66*).

Quantification and statistical analysis

Western blot quantification

Differential band density was quantified by ImageQuant TL software using area and profile-based toolbox. For glycerol gradient Western blot quantification, an area frame was defined for all bands (total CDK9 protein content in all fractions), and complex-bound CDK9 bands (heavy fractions) or free CDK9 bands (light fractions) were defined. The three area frames were measured for total density after background subtraction (local average). Relative complex-bound CDK9 or free CDK9 percentage was calculated regarding the untreated control (total CDK9 abundance). For RNAPII Ser^2 phosphorylation, CDK9 T-loop phosphorylation, or immunoprecipitation Western blot quantification, an area for each respective band and loading controls were defined, and total density was measured after background subtraction (local average). LARP7 abundance was first normalized to total CDK9 abundance for each lane, and relative abundance was calculated regarding untreated control. RNAPII Ser^2 abundance was first normalized to tubulin abundance for each lane, and relative abundance was calculated with respect to untreated control. Thr^{186} P-CDK9 and cyclin T1 band density was normalized to total CDK9 abundance, and relative abundance was calculated with respect to untreated control.

Statistical significance

Statistical significance was calculated as indicated in the figure legends. Analyses were performed using Prism version 7.03 (GraphPad software).

Data and code availability

Sequencing data that support the findings of this study were deposited in Gene Expression Omnibus and are available under the accession code GSE135184.

SUPPLEMENTARY MATERIALS

Supplementary material for this article is available at http://advances.sciencemag.org/cgi/content/full/6/33/eaba6617/DC1

View/request a protocol for this paper from *Bio-protocol*.

REFERENCES AND NOTES

1. D. D. Ho, A. U. Neumann, A. S. Perelson, W. Chen, J. M. Leonard, M. Markowitz, Rapid turnover of plasma virions and CD4 lymphocytes in HIV-1 infection. *Nature* **373**, 123–126 (1995).
2. A. S. Perelson, P. Essunger, Y. Cao, M. Vesanen, A. Hurley, K. Saksela, M. Markowitz, D. D. Ho, Decay characteristics of HIV-1-infected compartments during combination therapy. *Nature* **387**, 188–191 (1997).
3. X. Wei, S. K. Ghosh, M. E. Taylor, V. A. Johnson, E. A. Emini, P. Deutsch, J. D. Lifson, S. Bonhoeffer, M. A. Nowak, B. H. Hahn, M. S. Saag, G. M. Shaw, Viral dynamics in human immunodeficiency virus type 1 infection. *Nature* **373**, 117–122 (1995).
4. J. M. Siliciano, R. F. Siliciano, The Remarkable Stability of the Latent Reservoir for HIV-1 in Resting Memory $CD4^+$ T Cells. *J. Infect. Dis.* **212**, 1345–1347 (2015).
5. N. M. Archin, A. L. Liberty, A. D. Kashuba, S. K. Choudhary, J. D. Kuruc, A. M. Crooks, D. C. Parker, E. M. Anderson, M. F. Kearney, M. C. Strain, D. D. Richman, M. G. Hudgens, R. J. Bosch, J. M. Coffin, J. J. Eron, D. J. Hazuda, D. M. Margolis, Administration of vorinostat disrupts HIV-1 latency in patients on antiretroviral therapy. *Nature* **487**, 482–485 (2012).
6. T. A. Rasmussen, O. S. Søgaard, Clinical interventions in HIV cure research. *Adv. Exp. Med. Biol.* **1075**, 285–318 (2018).
7. A. M. Spivak, V. Planelles, Novel latency reversal agents for HIV-1 cure. *Annu. Rev. Med.* **69**, 421–436 (2018).
8. Y. Kim, J. L. Anderson, S. R. Lewin, Getting the "Kill" into "Shock and Kill": Strategies to eliminate latent HIV. *Cell Host Microbe* **23**, 14–26 (2018).
9. E. Battivelli, M. S. Dahabieh, M. Abdel-Mohsen, J. P. Svensson, I. T. D. Silva, L. B. Cohn, A. Gramatica, S. Deeks, W. C. Greene, S. K. Pillai, E. Verdin, Distinct chromatin functional states correlate with HIV latency reactivation in infected primary $CD4^+$ T cells. *eLife* **7**, e34655 (2018).
10. Y.-C. Ho, L. Shan, N. N. Hosmane, J. Wang, S. B. Laskey, D. I. S. Rosenbloom, J. Lai, J. N. Blankson, J. D. Siliciano, R. F. Siliciano, Replication-competent noninduced proviruses in the latent reservoir increase barrier to HIV-1 cure. *Cell* **155**, 540–551 (2013).
11. S. Bouchat, N. Delacourt, A. Kula, G. Darcis, B. Van Driessche, F. Corazza, J.-S. Gatot, A. Melard, C. Vanhulle, K. Kabeya, M. Pardons, V. Avettand-Fenoel, N. Clumeck, S. De Wit, O. Rohr, C. Rouzioux, C. Van Lint, Sequential treatment with 5-aza-2′-deoxycytidine and deacetylase inhibitors reactivates HIV-1. *EMBO Mol. Med.* **8**, 117–138 (2016).
12. R. B. Jones, R. O'Connor, S. Mueller, M. Foley, G. L. Szeto, D. Karel, M. Lichterfeld, C. Kovacs, M. A. Ostrowski, A. Trocha, D. J. Irvine, B. D. Walker, Histone deacetylase inhibitors impair the elimination of HIV-infected cells by cytotoxic T-lymphocytes. *PLOS Pathog.* **10**, e1004287 (2014).
13. M. Zhao, E. De Crignis, C. Rokx, A. Verbon, T. van Gelder, T. Mahmoudi, P. D. Katsikis, Y. M. Mueller, T cell toxicity of HIV latency reversing agents. *Pharmacol. Res.* **139**, 524–534 (2019).
14. D. J. Newman, G. M. Cragg, Natural products as sources of new drugs from 1981 to 2014. *J. Nat. Prod.* **79**, 629–661 (2016).
15. J. F. Sanchez, A. D. Somoza, N. P. Keller, C. C. C. Wang, Advances in *Aspergillus* secondary metabolite research in the post-genomic era. *Nat. Prod. Rep.* **29**, 351–371 (2012).
16. A. A. Brakhage, Regulation of fungal secondary metabolism. *Nat. Rev. Microbiol.* **11**, 21–32 (2013).
17. J. Přichystal, K. A. Schug, K. Lemr, J. Novák, V. Havlíček, Structural analysis of natural products. *Anal. Chem.* **88**, 10338–10346 (2016).
18. E. Ne, R.-J. Palstra, T. Mahmoudi, Transcription: Insights from the HIV-1 promoter. *Int. Rev. Cell Mol. Biol.* **335**, 191–243 (2018).
19. M. Stoszko, E. Ne, E. Abner, T. Mahmoudi, A broad drug arsenal to attack a strenuous latent HIV reservoir. *Curr. Opin. Virol.* **38**, 37–53 (2019).
20. J. Novák, L. Sokolová, K. Lemr, T. Pluháček, A. Palyzová, V. Havlíček, Batch-processing of imaging or liquid-chromatography mass spectrometry datasets and *De Novo* sequencing of polyketide siderophores. *Biochim. Biophys. Acta. Proteins Proteom.* **1865**, 768–775 (2017).
21. K. G. Lassen, A. M. Hebbeler, D. Bhattacharyya, M. A. Lobritz, W. C. Greene, A flexible model of HIV-1 latency permitting evaluation of many primary CD4 T-cell reservoirs. *PLOS ONE.* **7**, e30176 (2012).
22. M. Stanzani, E. Orciuolo, R. Lewis, D. P. Kontoyiannis, S. L. R. Martins, L. S. S. John, K. V. Komanduri, *Aspergillus fumigatus* suppresses the human cellular immune response via gliotoxin-mediated apoptosis of monocytes. *Blood* **105**, 2258–2265 (2005).
23. Y. K. Suen, K. P. Fung, C. Y. Lee, S. K. Kong, Gliotoxin induces apoptosis in cultured macrophages via production of reactive oxygen species and cytochrome c release without mitochondrial depolarization. *Free Radic. Res.* **35**, 1–10 (2001).
24. A. Yamada, T. Kataoka, K. Nagai, The fungal metabolite gliotoxin: Immunosuppressive activity on CTL-mediated cytotoxicity. *Immunol. Lett.* **71**, 27–32 (2000).
25. D. H. Scharf, A. A. Brakhage, P. K. Mukherjee, Gliotoxin--bane or boon? *Environ. Microbiol.* **18**, 1096–1109 (2016).
26. L. Trautmann, Kill: Boosting HIV-specific immune responses. *Curr. Opin. HIV AIDS* **11**, 409–416 (2016).
27. M. Stoszko, E. De Crignis, C. Rokx, M. M. Khalid, C. Lungu, R.-J. Palstra, T. W. Kan, C. Boucher, A. Verbon, E. C. Dykhuizen, T. Mahmoudi, Small molecule inhibitors of BAF; A promising family of compounds in HIV-1 latency reversal. *EBioMedicine* **3**, 108–121 (2016).

28. C. A. Marian, M. Stoszko, L. Wang, M. W. Leighty, E. de Crignis, C. A. Maschinot, J. Gatchalian, B. C. Carter, B. Chowdhury, D. C. Hargreaves, J. R. Duvall, G. R. Crabtree, T. Mahmoudi, E. C. Dykhuizen, Small molecule targeting of specific BAF (mSWI/SNF) complexes for HIV latency reversal. *Cell Chem. Biol.* **25**, 1443–55.e14 (2018).
29. A. J. C. Quaresma, A. Bugai, M. Barboric, Cracking the control of RNA polymerase II elongation by 7SK snRNP and P-TEFb. *Nucleic Acids Res.* **44**, 7527–7539 (2016).
30. V. T. Nguyen, T. Kiss, A. A. Michels, O. Bensaude, 7SK small nuclear RNA binds to and inhibits the activity of CDK9/cyclin T complexes. *Nature* **414**, 322–325 (2001).
31. E. Uchikawa, K. S. Natchiar, X. Han, F. Proux, P. Roblin, E. Zhang, A. Durand, B. P. Klaholz, A.-C. Dock-Bregeon, Structural insight into the mechanism of stabilization of the 7SK small nuclear RNA by LARP7. *Nucleic Acids Res.* **43**, 3373–3388 (2015).
32. Z. Yang, Q. Zhu, K. Luo, Q. Zhou, The 7SK small nuclear RNA inhibits the CDK9/cyclin T1 kinase to control transcription. *Nature* **414**, 317–322 (2001).
33. J. H. N. Yik, R. Chen, R. Nishimura, J. L. Jennings, A. J. Link, Q. Zhou, Inhibition of P-TEFb (CDK9/Cyclin T) kinase and RNA polymerase II transcription by the coordinated actions of HEXIM1 and 7SK snRNA. *Mol. Cell* **12**, 971–982 (2003).
34. M. Ott, M. Geyer, Q. Zhou, The control of HIV transcription: Keeping RNA polymerase II on track. *Cell Host Microbe* **10**, 426–435 (2011).
35. G. Mousseau, S. T. Valente, Role of host factors on the regulation of Tat-Mediated HIV-1 transcription. *Curr. Pharm. Des.* **23**, 4079–4090 (2017).
36. B. M. Peterlin, D. H. Price, Controlling the elongation phase of transcription with P-TEFb. *Mol. Cell* **23**, 297–305 (2006).
37. I. Jonkers, J. T. Lis, Getting up to speed with transcription elongation by RNA polymerase II. *Nat. Rev. Mol. Cell Biol.* **16**, 167–177 (2015).
38. S. A. Yukl, P. Kaiser, P. Kim, S. Telwatte, S. K. Joshi, M. Vu, H. Lampiris, J. K. Wong, HIV latency in isolated patient $CD4^+$ T cells may be due to blocks in HIV transcriptional elongation, completion, and splicing. *Sci. Transl. Med.* **10**, eaap9927 (2018).
39. U. Mbonye, J. Karn, The molecular basis for human immunodeficiency virus latency. *Annu. Rev. Virol.* **4**, 261–285 (2017).
40. R. Ramakrishnan, E. C. Dow, A. P. Rice, Characterization of Cdk9 T-loop phosphorylation in resting and activated $CD4^+$ T lymphocytes. *J. Leukoc. Biol.* **86**, 1345–1350 (2009).
41. B. J. Krueger, C. Jeronimo, B. B. Roy, A. Bouchard, C. Barrandon, S. A. Byers, C. E. Searcey, J. J. Cooper, O. Bensaude, E. A. Cohen, B. Coulombe, D. H. Price, LARP7 is a stable component of the 7SK snRNP while P-TEFb, HEXIM1 and hnRNP A1 are reversibly associated. *Nucleic Acids Res.* **36**, 2219–2229 (2008).
42. E. Abner, M. Stoszko, L. Zeng, H.-C. Chen, A. Izquierdo-Bouldstridge, T. Konuma, E. Zorita, E. Fanunza, Q. Zhang, T. Mahmoudi, M.-M. Zhou, G. J. Filion, A. Jordan, A new quinoline BRD4 inhibitor targets a distinct latent HIV-1 reservoir for reactivation from other "Shock" drugs. *J. Virol.* **92**, (2018).
43. H.-C. Chen, J. P. Martinez, E. Zorita, A. Meyerhans, G. J. Filion, Position effects influence HIV latency reversal. *Nat. Struct. Mol. Biol.* **24**, 47–54 (2017).
44. E. Abner, A. Jordan, HIV "shock and kill" therapy: In need of revision. *Antiviral Res.* **166**, 19–34 (2019).
45. G. Darcis, A. Kula, S. Bouchat, K. Fujinaga, F. Corazza, A. Ait-Ammar, N. Delacourt, A. Melard, K. Kabeya, C. Vanhulle, B. Van Driessche, J.-S. Gatot, T. Cherrier, L. F. Pianowski, L. Gama, C. Schwartz, J. Vila, A. Burny, N. Clumeck, M. Moutschen, S. De Wit, B. M. Peterlin, C. Rouzioux, O. Rohr, C. Van Lint, An in-depth comparison of latency-reversing agent combinations in various *In Vitro* and *Ex Vivo* HIV-1 Latency Models Identified Bryostatin-1+JQ1 and Ingenol-B+JQ1 to Potently Reactivate Viral Gene Expression. *PLOS Pathog.* **11**, e1005063 (2015).
46. P. Hashemi, K. Barreto, W. Bernhard, A. Lomness, N. Honson, T. A. Pfeifer, P. R. Harrigan, I. Sadowski, Compounds producing an effective combinatorial regimen for disruption of HIV-1 latency. *EMBO Mol. Med.* **10**, 160–174 (2018).
47. G. M. Laird, C. K. Bullen, D. I. S. Rosenbloom, A. R. Martin, A. L. Hill, C. M. Durand, J. D. Siliciano, R. F. Siliciano, Ex vivo analysis identifies effective HIV-1 latency-reversing drug combinations. *J. Clin. Invest.* **125**, 1901–1912 (2015).
48. T. A. Rasmussen, S. R. Lewin, Shocking HIV out of hiding: Where are we with clinical trials of latency reversing agents? *Curr. Opin. HIV AIDS* **11**, 394–401 (2016).
49. H. Rafati, M. Parra, S. Hakre, Y. Moshkin, E. Verdin, T. Mahmoudi, Repressive LTR nucleosome positioning by the BAF complex is required for HIV latency. *PLOS Biol.* **9**, e1001206 (2011).
50. X. Contreras, M. Barboric, T. Lenasi, B. M. Peterlin, HMBA releases P-TEFb from HEXIM1 and 7SK snRNA via PI3K/Akt and activates HIV transcription. *PLOS Pathog.* **3**, 1459–1469 (2007).
51. J. Kohoutek, P-TEFb- the final frontier. *Cell Div.* **4**, 19 (2009).
52. H. S. Choi, J. S. Shim, J.-A. Kim, S. W. Kang, H. J. Kwon, Discovery of gliotoxin as a new small molecule targeting thioredoxin redox system. *Biochem. Biophys. Res. Commun.* **359**, 523–528 (2007).
53. K. J. Kwon-Chung, J. A. Sugui, What do we know about the role of gliotoxin in the pathobiology of *Aspergillus fumigatus*? *Med. Mycol.* **47**, (suppl. 1), S97–S103 (2009).
54. H. Sakamoto, S. Egashira, N. Saito, T. Kirisako, S. Miller, Y. Sasaki, T. Matsumoto, M. Shimonishi, T. Komatsu, T. Terai, T. Ueno, K. Hanaoka, H. Kojima, T. Okabe, S. Wakatsuki, K. Iwai, T. Nagano, Gliotoxin suppresses NF-κB activation by selectively inhibiting linear ubiquitin chain assembly complex (LUBAC). *ACS Chem. Biol.* **10**, 675–681 (2015).
55. G. Wichmann, O. Herbarth, I. Lehmann, The mycotoxins citrinin, gliotoxin, and patulin affect interferon-γ rather than interleukin-4 production in human blood cells. *Environ. Toxicol.* **17**, 211–218 (2002).
56. R. E. Lewis, N. P. Wiederhold, J. Chi, X. Y. Han, K. V. Komanduri, D. P. Kontoyiannis, R. A. Prince, Detection of gliotoxin in experimental and human aspergillosis. *Infect. Immun.* **73**, 635–637 (2005).
57. C. Gostinčar, J. Zajc, M. Lenassi, A. Plemenitaš, S. de Hoog, A. M. S. Al-Hatmi, N. Gunde-Cimerman, Fungi between extremotolerance and opportunistic pathogenicity on humans. *Fungal Diversity.* **93**, 195–213 (2018).
58. C. A. Spina, J. Anderson, N. M. Archin, A. Bosque, J. Chan, M. Famiglietti, W. C. Greene, A. Kashuba, S. R. Lewin, D. M. Margolis, M. Mau, D. Ruelas, S. Saleh, K. Shirakawa, R. F. Siliciano, A. Singhania, P. C. Soto, V. H. Terry, E. Verdin, C. Woelk, S. Wooden, S. Xing, V. Planelles, An in-depth comparison of latent HIV-1 reactivation in multiple cell model systems and resting CD4+ T cells from aviremic patients. *PLOS Pathog.* **9**, e1003834 (2013).
59. T. D. Schmittgen, K. J. Livak, Analyzing real-time PCR data by the comparative C_T method. *Nat. Protoc.* **3**, 1101–1108 (2008).
60. A. J. Link, J. LaBaer, Trichloroacetic acid (TCA) precipitation of proteins. *Cold Spring Harb. Protoc.* **2011**, 993–994 (2011).
61. K. Bartholomeeusen, Y. Xiang, K. Fujinaga, B. M. Peterlin, Bromodomain and extra-terminal (BET) bromodomain inhibition activate transcription via transient release of positive transcription elongation factor b (P-TEFb) from 7SK small nuclear ribonucleoprotein. *J. Biol. Chem.* **287**, 36609–36616 (2012).
62. R. P. Joosten, F. Long, G. N. Murshudov, A. Perrakis, The *PDB_REDO* server for macromolecular structure model optimization. *IUCrJ.* **1**, (Pt. 4), 213–220 (2014).
63. C. D. Eichhorn, Y. Yang, L. Repeta, J. Feigon, Structural basis for recognition of human 7SK long noncoding RNA by the La-related protein Larp7. *Proc. Natl. Acad. Sci. U.S.A.* **115**, E6457–E6466 (2018).
64. E. F. Pettersen, T. D. Goddard, C. C. Huang, G. S. Couch, D. M. Greenblatt, E. C. Meng, T. E. Ferrin, UCSF Chimera--a visualization system for exploratory research and analysis. *J. Comput. Chem.* **25**, 1605–1612 (2004).
65. O. Trott, A. J. Olson, AutoDock Vina: Improving the speed and accuracy of docking with a new scoring function, efficient optimization, and multithreading. *J. Comput. Chem.* **31**, 455–461 (2010).
66. L. Schrödinger, The {PyMOL} Molecular Graphics System, Version 1.8 (2015).

Acknowledgments

Funding: T.M. received funding from the European Research Council (ERC) under the European Union's Seventh Framework Programme (FP/2007-2013)/ERC STG 337116 Trxn-PURGE, the Dutch AIDS Fonds grant 2014021, and Erasmus MC mRACE research grant. J.K. was supported by the Technology Innovation Team Project of Guiyang [20161001]005; Guiyang Science and Technology Project (2017) No.5-19. V.H. was supported by the Ministry of Education, Youth, and Sports of the Czech Republic (LO 1509). R.P. was supported by the Dutch AIDS Fonds grant. 2016014. J.H.G.L. is supported by the gravitation program CancerGenomiCs.nl from the Netherlands Organization for Scientific Research (NWO). P.D.K. was supported in part by a grant awarded by Worldwide Cancer Research. **Author contributions:** M.St., A.M.S.A.-H., A.S., M.R., E.N., Y.M.M., M.J.N., R.C., J.K., R.P., E.L., P.B., A.B., T.W.K., E.d.C., R.-J.P., M.Su., C.R., and W.v.I. conducted the experiments. M.St., Y.M.M., R.-J.P., J.H.G.L., A.V., P.D.K., V.H., S.d.H., and T.M. designed the experiments and wrote the paper. **Competing interests:** The authors declare that they have no competing interests. **Data and materials availability:** All data needed to evaluate the conclusions in the paper are present in the paper and/or the Supplementary Materials. Additional data related to this paper may be requested from the authors.

Submitted 20 December 2019
Accepted 1 July 2020
Published 12 August 2020
10.1126/sciadv.aba6617

Citation: M. Stoszko, A. M. S. Al-Hatmi, A. Skriba, M. Roling, E. Ne, R. Crespo, Y. M. Mueller, M. J. Najafzadeh, J. Kang, R. Ptackova, E. LeMasters, P. Biswas, A. Bertoldi, T. W. Kan, E. de Crignis, M. Sulc, J. H. Lebbink, C. Rokx, A. Verbon, W. van Ijcken, P. D. Katsikis, R.-J. Palstra, V. Havlicek, S. de Hoog, T. Mahmoudi, Gliotoxin, identified from a screen of fungal metabolites, disrupts 7SK snRNP, releases P-TEFb, and reverses HIV-1 latency. *Sci. Adv.* **6**, eaba6617 (2020).

Science Advances

Gliotoxin, identified from a screen of fungal metabolites, disrupts 7SK snRNP, releases P-TEFb, and reverses HIV-1 latency

Mateusz Stoszko, Abdullah M. S. Al-Hatmi, Anton Skriba, Michael Roling, Enrico Ne, Raquel Crespo, Yvonne M. Mueller, Mohammad Javad Najafzadeh, Joyce Kang, Renata Ptackova, Elizabeth LeMasters, Pritha Biswas, Alessia Bertoldi, Tsung Wai Kan, Elisa de Crignis, Miroslav Sulc, Joyce H.G. Lebbink, Casper Rokx, Annelies Verbon, Wilfred van Ijcken, Peter D. Katsikis, Robert-Jan Palstra, Vladimir Havlicek, Sybren de Hoog and Tokameh Mahmoudi

Sci Adv **6** (33), eaba6617.
DOI: 10.1126/sciadv.aba6617

Science Advances (ISSN 2375-2548) is published by the American Association for the Advancement of Science, 1200 New York Avenue NW, Washington, DC 20005. The title *Science Advances* is a registered trademark of AAAS.